Title

Iron-dependent modifications of the flower transcriptome, proteome, metabolome, and hormonal content in an Arabidopsis ferritin mutant

Journal

Journal of Experimental Botany, 64(10)

ISSN

0022-0957

Authors

Sudre, Damien
Gutierrez-Carbonell, Elain
Lattanzio, Giuseppe
et al.

Publication Date

2013-07-01

DOI

10.1093/jxb/ert112

Peer reviewed

Journal of Experimental Botany, Vol. 64, No. 10, pp. 2665–2688, 2013
doi:10.1093/jxb/ert112 Advance Access publication 16 May, 2013
This paper is available online free of all access charges (see http://jxb.oxfordjournals.org/open_access.html for further details)

Journal of Experimental Botany
www.jxb.oxfordjournals.org

RESEARCH PAPER

Iron-dependent modifications of the flower transcriptome, proteome, metabolome, and hormonal content in an *Arabidopsis* ferritin mutant

Damien Sudre[1,*], Elain Gutierrez-Carbonell[2,*], Giuseppe Lattanzio[2], Rubén Rellán-Álvarez[2,†], Frédéric Gaymard[1], Gert Wohlgemuth[3], Oliver Fiehn[3], Ana Álvarez-Fernández[2], Angel M. Zamarreño[4], Eva Bacaicoa[4], Daniela Duy[5], Jose-María García-Mina[4], Javier Abadía[2], Katrin Philippar[5], Ana-Flor López-Millán and Jean-François Briat[1,‡]

[1] Biochimie et Physiologie Moléculaire des Plantes, Centre National de la Recherche Scientifique, Institut National de la Recherche Agronomique, Université Montpellier 2, SupAgro. Bat 7, 2 place Viala, 34060 Montpellier cedex 1, France
[2] Department of Plant Nutrition, Estación Experimental de Aula Dei (CSIC), Av. Montañana 1005, E-50080 Zaragoza, Spain
[3] Department of Molecular and Cellular Biology & Genome Center, University of California, Davis, Health Sciences Drive, Davis, CA 95616, USA
[4] CIPAV, Timac Agro España, Poligono Arazuri-Orcoyen, Calle C, no. 32, E-31160 Orcoyen, Spain
[5] Ludwig-Maximilians-University (LMU) München, Department Biology I, Plant Biochemistry and Physiology, Großhaderner Str. 2–4, D-82152 Planegg-Martinsried, Germany

*These authors contributed equally to this work.
†Present address: Department of Plant Biology, Carnegie Institution for Science, Stanford, CA 94305, USA.
‡ To whom correspondence should be addressed. E-mail: briat@supagro.inra.fr

Received 8 December 2012; Revised 14 March 2013; Accepted 26 March 2013

Abstract

Iron homeostasis is an important process for flower development and plant fertility. The role of plastids in these processes has been shown to be essential. To document the relationships between plastid iron homeostasis and flower biology further, a global study (transcriptome, proteome, metabolome, and hormone analysis) was performed of *Arabidopsis* flowers from wild-type and triple *atfer1-3-4* ferritin mutant plants grown under iron-sufficient or excess conditions. Some major modifications in specific functional categories were consistently observed at these three omic levels, although no significant overlaps of specific transcripts and proteins were detected. These modifications concerned redox reactions and oxidative stress, as well as amino acid and protein catabolism, this latter point being exemplified by an almost 10-fold increase in urea concentration of *atfer1-3-4* flowers from plants grown under iron excess conditions. The mutant background caused alterations in Fe–haem redox proteins located in membranes and in hormone-responsive proteins. Specific effects of excess Fe in the mutant included further changes in these categories, supporting the idea that the mutant is facing a more intense Fe/redox stress than the wild type. The mutation and/or excess Fe had a strong impact at the membrane level, as denoted by the changes in the transporter and lipid metabolism categories. In spite of the large number of genes and proteins responsive to hormones found to be regulated in this study, changes in the hormonal balance were restricted to cytokinins, especially in the mutant plants grown under Fe excess conditions.

Key words: Ferritin, flowers, functional genomics, iron.

Introduction

Flower development and plant fertility are dependent on iron homeostasis (Takahashi *et al.*, 2003). Small organic molecules such as nicotianamine (NA) and citrate participate in this process by chelating Fe in order to shuttle it throughout the plant (Curie *et al.*, 2009; Rellán-Álvarez *et al.*, 2010; Schuler *et al.*, 2012). Overexpressing the barley nicotianamine

amino transferase (NAAT) in transgenic tobacco depletes the NA pools of these plants, leading to abnormally shaped and sterile flowers (Takahashi *et al.*, 2003). NA–Fe(II) complexes are transported by members of the *YSL* gene family (Curie *et al.*, 2009; Conte and Walker, 2011). Among them, it is well established that the *YSL1* and *YSL3* genes are required for fertility of *Arabidopsis* flowers, and that pollen function is severely reduced in a *ysl1ysl3* double knockout mutant (Le Jean *et al.*, 2005; Waters *et al.*, 2006). Citrate, as an Fe chelator, also appears to be crucial for flower development and fertility (Roschzttardtz *et al.*, 2011). The *FRD3* gene encodes a citrate effluxer (Durrett *et al.*, 2007). Flowers from a null *frd3* allele have an altered anther structure, and lack pollen grain at the anther surface (Roschzttardtz *et al.*, 2011). These studies have clearly demonstrated that long-distance Fe trafficking and its correct allocation within reproductive organs are essential for flower development and fertility.

At the subcellular level, chloroplast Fe homeostasis has also recently been linked to flower development and fertility. *Arabidopsis* PIC1 (permease in chloroplast1) is an intrinsic membrane protein located at the chloroplast inner envelope, and is involved in Fe uptake by plastids (Duy *et al.*, 2007). Flowers of PIC1 overexpressor (PIC1ox) plants showed impaired development, elevated Fe levels, and reprogramming of their genome expression (Duy *et al.*, 2011). Whereas the latter phenotype (PIC1ox) resembled that of ferritin knockouts (see below), *pic1* knockout mutants accumulated ferritin in plastids (Duy *et al.*, 2007). Plant ferritins are Fe storage proteins playing a key role in oxidative stress defence (Ravet *et al.*, 2009*a*; Briat *et al.*, 2010*a*, *b*). In *Arabidopsis*, flower development of *atfer1-3-4* triple ferritin mutant plants is impaired and fertility decreased. Flowers of this mutant overaccumulate Fe and have their reactive oxygen species (ROS)-scavenging mechanisms activated. Furthermore, the absence of ferritin in this mutant led to a strong deregulation of the expression of 24 genes encoding metal transporters in flowers and stems, including the *PIC1* gene (Ravet *et al.*, 2009*a*).

The extent to which the impact of Fe homeostasis on plant development is communicated by plant hormones also needs to be considered. Indeed, the interactions between Fe metabolism and plant hormones have received increased attention in the last few years (Romera *et al.*, 2011). Auxin, ethylene, and nitric oxide (NO) increased in Fe-deficient plants in relation to the up-regulation of root Fe acquisition genes (Bacaicoa *et al.*, 2011; Lingam *et al.*, 2011), whereas jasmonate was found to suppress this gene induction (Maurer *et al.*, 2011). Auxin also plays a role in lateral root elongation regulated by local Fe concentrations (Giehl *et al.*, 2012), and abscisic acid (ABA) plays a role in the regulation of some ferritin genes in response to Fe excess (Lobreaux *et al.*, 1993).

The main aim of this study was to document the roles that Fe homeostasis plays in flower development and fertility, in particular when plastid Fe homeostasis is altered. To attain this goal, transcriptomic, proteomic, and metabolomic analysis were performed, and hormone concentrations were determined, on the same samples of *Arabidopsis* flowers collected from wild-type (WT) and triple *atfer1-3-4* mutant plants grown under standard or Fe excess conditions. This approach enables the description of the impact of the perturbed Fe homeostasis caused by the loss of ferritin and/or iron overload at various molecular levels in flowers. In addition, the study provides a start for generating a coherent scheme of the role that ferritins play in flower biology.

Materials and methods

Plant materials, growth conditions, and sampling of flowers

Arabidopsis Columbia (Col-0) and the previously described mutant line *atfer1-3-4* (Ravet *et al.*, 2009*a*) were sown on soil (Humin substrate N2) in pots as single plants and kept at 4 °C for 2 d prior to being grown in a growth chamber under long-day conditions (16 h light/8 h dark, 23 °C). Plants were irrigated once a week with reverse osmosis water without Fe added (standard soil) (WT and *atfer1-3-4*), or supplemented with Fe excess (2 mM Fe-EDDHA) (WT++ and *atfer1-3-4*++).

Flowers were harvested as a mix of development stages 1 and 2, as previously defined (Ravet *et al.*, 2009*b*), six times every 2 d on 10 individuals from 4-week-old *atfer1-3-4* mutant and WT plants. Flowers were immediately frozen in liquid nitrogen after harvest. To guarantee comparability of data, all flower samples were produced under the same conditions in the same growth chamber of only one laboratory (Montpellier). Frozen flower samples, RNA, and proteins were then dispatched from the Montpellier laboratory to other laboratories (München, Zaragoza, Davis, and CIPAV) for transcriptomics, proteomics, metabolomics, and hormone dosage, respectively.

RNA extraction and transcriptome analysis

Flowers from different plants (collected three times from 10 individuals each) and grown with and without Fe excess were ground in liquid nitrogen. RNAs were extracted using an RNeasy Mini Kit (Qiagen). For microarray analysis, 5 µg of RNA from flowers of the *atfer1-3-4* mutant and the WT were processed and hybridized to Affymetrix GeneChip Arabidopsis ATH1 Genome Arrays as described in Duy *et al.* (2011). For quality check and normalization, raw intensity values were processed with Robin software (Lohse *et al.*, 2010) default settings. Specifically, for background correction, the robust multiarray average normalization method (Irizarry *et al.*, 2003) was performed across all arrays (between-array method). Statistical analysis of differential gene expression of *atfer1-3-4* versus WT flowers was carried out using the linear model-based approach developed by Smyth (2004). Thereby, differential clustering of n=2 replicates, each representing pooled tissue of 10 individual plants, was obtained. The obtained P-values were corrected for multiple testing using the nestedF procedure, applying a significance threshold of 0.10 for mutant versus the WT and 0.20 for Fe excess versus Fe-sufficient comparisons, in combination with the Benjamini and Hochberg (1995) false discovery rate control. To verify differential expression, the transcript content of 12 representative genes, classified as regulated by microarrays (Tables 1–3), was re-analysed by quantitative real-time reverse transcription–PCR (qRT–PCR; Supplementary Table S1 available at *JXB* online). Because here only one gene for one comparison showed deviating behaviour, micorarray data were considered as robust.

Protein extraction

Flowers from different plants were ground in a mortar in liquid nitrogen, and the ground material was stored at –80 °C. The flower powder (~1 g) was resuspended in 2 ml Eppendorf tubes using 1 ml of 10% trichloroacetic acid (TCA), 0.07% β-mercaptoethanol in acetone, incubated for 45 min at –20°C (shaking at 5, 10, and

Table 1. Genes significantly regulated in all three comparisons of *atfer1-3-4* mutants versus Col-0 wild type (WT) under Fe-sufficient and Fe excess (++) conditions. The 54 genes common in the comparisons *atfer1-3-4* versus WT, *atfer1-3-4*++ versus WT, and *atfer1-3-4*++ versus WT++ (Fig. 1A) are classified into functional categories. The fold change of the transcript content is given for each comparison. Bold characters in fold changes indicate adjusted *P*-values <0.05; those not in bold indicate 0.05 < *P* < 0.1. The AGI codes, names, annotated functions, and/or domains, as well as metal binding of the corresponding proteins are listed. Genes that were also regulated in flowers of PIC1 overexpressors (Duy *et al.*, 2011) are highlighted by a grey background; those that were re-analysed by qRT–PCR (Supplementary Table S1 at *JXB* online) are underlined.

AGI code		*atfer1-3-4* versus WT	*atfer1-3-4*++ versus WT	*atfer1-3-4*++ versus WT++	Name, function/domains	Metal binding
At5g01600	Iron homeostasis	***–138.6***	**–160.2**	**–157.0**	FER1, ferritin	Fe
At2g40300		***–15.5***	**–15.8**	**–17.9**	FER4, ferritin	Fe
AtCg00050	Protein metabolism +modification	*4.3*	**14.1**	**7.2**	*RPS16*, chloroplast ribosomal protein S16	
At1g14370		*1.6*	**1.9**	**1.9**	APK2A, receptor-like protein kinase	
At2g42360		*1.7*	**2.0**	1.8	Ubiquitin protein ligase/zinc finger protein	Zn
At1g02850	Carbohydrate metabolism	*1.9*	**2.2**	1.9	BGLU11, beta glucosidase	
At2g27690	Lipid metabolism	*–1.4*	**–1.6**	**–1.7**	CYP94C1, fatty acid-hydroxylase/ cytochrome P450	Fe–haem
At4g12490		***7.2***	**3.7**	**4.7**	Protease inhibitor/seed storage/lipid transfer protein (LTP)	
At2g23540		*–1.7*	**–1.6**	**–1.7**	GDSL-motif lipase/hydrolase family protein	
At2g38870	Stress+redox	***3.0***	**2.7**	**2.6**	Protease inhibitor, putative/pathogenesis-related peptide/wounding	
At3g54420		*2.0*	1.8	1.7	ATEP3, chitinase/hypersensitive response/ embryogenesis	
At5g06320		***1.7***	**1.9**	1.4	NHL3, involved in defence response	
At1g07890		*1.4*	**1.6**	1.4	APX1, ascorbate peroxidase 1	Fe–haem
At1g26380		*4.4*	3.8	**4.2**	FAD-binding berberine family/electron carrier, oxidoreductase	
At1g26390		***16.0***	**17.3**	**19.6**	FAD-binding berberine family/electron carrier, *oxidoreductase*	
At1g26410		*2.6*	1.9	**2.8**	FAD-binding berberine family/electron carrier, oxidoreductase	
At3g09270		***4.0***	**3.0**	**2.8**	ATGSTU8, glutathione *S*-transferase tau8	
At2g30750		*3.1*	2.8	3.5	CYP71A12, cytochrome P450 family monooxygenase	Fe–haem
At3g26210		*2.0*	2.1	**2.8**	CYP71B23, cytochrome P450 family monooxygenase	Fe–haem
At4g31970		***10.0***	**17.4**	**16.8**	*CYP82C2*, cytochrome P450 family monooxygenase	Fe–haem
At4g37370		*4.0*	**4.5**	**4.0**	CYP81D8, cytochrome P450 family monooxygenase	Fe–haem e
At1g33660		*1.4*	**1.7**	1.5	Peroxidase family protein	Fe–haem
At4g36430		*2.0*	**2.0**	1.8	Peroxidase family protein	Fe–haem
At3g20340		*3.3*	**4.4**	3.9	Molecular function unknown/response to oxidative stress	
At5g46350	DNA/RNA processes	2.2	**2.3**	**2.2**	WRKY8, transcription factor, response to H_2O_2	

Table 1. *Continued.*

AGI code		*atfer1-3-4* versus WT	*atfer1-3-4*++ versus WT	*atfer1-3-4*++ versus WT++	Name, function/domains	Metal binding
At2g44430		**–3.1**	**–3.5**	**–4.3**	DNA-binding/bromodomain-containing protein	
At1g53490		–1.9	–1.8	**–1.9**	DNA binding	
At4g08110		1.4	1.4	**1.6**	CACTA-like transposase	
At2g43000		**3.2**	**2.7**	**3.1**	ANAC042, transcription factor/NAC domain protein 42, induced by H_2O_2	
At5g06860	Cell wall modification	1.6	1.6	1.4	PGIP1, polygalacturonase-inhibiting protein 1	
At5g57560		1.4	–1.4	–1.5	TCH4, glycosyl hydrolase/ xyloglucan:xyloglucosyl transferase	
At5g42560	Hormone metabolism	**3.0**	**3.0**	**3.5**	Abscisic acid-responsive HVA22 family protein	
At3g17600		–1.4	1.3	–1.6	*IAA31*, transcription factor auxin reponse	
At1g36060		1.5	**1.6**	**1.7**	AP2-domain (apetala), ethylene-responsive transcription factor	
At3g50260		1.5	1.5	1.5	CEJ1, transcription factor/regulated by ethylene and jasmonate	
At5g24160		1.8	**4.0**	**4.9**	*SQE6*, FAD binding/squalene monooxygenase/ brassinosteroids	
At1g05680		1.6	**1.9**	1.5	UDP-glucoronosyl/-glucosyl transferase	
At4g33070	Others	**–2.1**	**–2.1**	**–1.9**	Thiamine pyrophosphate-dependent pyruvate decarboxylase family	Mg
At2g39330		1.6	**1.7**	**1.7**	JAL23, lectin	
At5g48850		–1.9	**–2.2**	–1.6	ATSDI1, sulphur deficiency-induced/ tetratricopeptide repeat domain	
At2g26400		–1.8	**–2.6**	–2.6	ATARD3, acireductone Fe(II)-dioxygenase/ heteroglycan binding	Fe
At2g25440	Signalling	2.3	**2.2**	**2.5**	AtRLP20, receptor like protein kinase	
At4g27280		1.3	–1.4	–1.4	Calcium-binding EF hand family protein	Ca
At5g49480		1.6	**2.2**	**2.3**	ATCP1, Ca^{2+}-binding protein	Ca
At1g12110	Transport	**1.8**	**1.9**	**1.9**	NRT1.1, nitrate transmembrane transporter	
At3g46980		**2.1**	**2.1**	**2.0**	PHT4;3, phosphate transporter-related	
At1g59590	Unknown function	1.7	1.5	1.5	ZCF37, molecular function unknown	
At2g17740		1.8	1.8	**1.9**	DC1 domain-containing protein/molecular function unknown	
At4g38080		–1.7	–1.7	**–1.9**	Hydroxyproline-rich glycoprotein family/ molecular function unknown	
At1g48300		–2.8	**–4.0**	**–3.2**	Molecular function unknown	
At1g76600		1.5	1.4	1.3	Molecular function unknown	
At3g45730		1.4	**1.6**	**1.9**	Molecular function unknown	
At4g36500		1.3	–1.5	–1.4	Molecular function unknown	
At5g05250		–1.5	**–1.5**	–1.4	Molecular function unknown	

Table 2. Genes significantly regulated only in the atfer *1-3-4*++ versus WT++ comparison. The 74 genes which are differentially expressed only in the *atfer1-3-4*++ versus WT++ comparison (see Fig. 1A) are classified into functional categories. The fold change of transcript content is given. Bold characters in fold changes indicate adjusted *P*-values <0.05; those not in bold indicate 0.05 < *P* < 0.1. The AGI codes, names, annotated functions, and/or domains, as well as metal binding of the corresponding proteins are listed. The column WT++ versus WT indicates regulation of genes in response to Fe excess in wild-type flowers (Fig. 1B). Genes that were also regulated in flowers of PIC1 overexpressors (Duy *et al.*, 2011) are highlighted by a grey background; those that were re-analysed by qRT–PCR (Supplementary Table S1 at *JXB* online) are underlined.

AGI code		*atfer1-3-4*++ versus WT++	WT++ versus WT	Name, function/domains	Metal binding
At1g23020	Iron homeostasis	1.4		*FRO3*, ferric-chelate reductase	Fe
At2g17360	Protein metabolism+modification	–1.3		RPS4A, 40S ribosomal protein S4	
At5g48650		–1.5		NTF2, nuclear transport factor 2 family protein/RNA recognition motif (RRM)	
At5g47350		–2.7		Palmitoyl protein thioesterase family protein	
At4g11890		2.6		Protein kinase family protein	
At5g58820		–1.6		Subtilisin-like serine endopeptidase family protein	
At5g58840		–1.8		Subtilisin-like serine endopeptidase family protein	
At4g12910		–1.4		scpl20, serine carboxypeptidase-like 20	
At1g13700	Carbohydrate metabolism	1.5		Glucosamine/galactosamine-6-phosphate isomerase family protein	
At1g19610	Stress+redox	2.0		LCR78, PDF1.4, pathogenesis-related protein/plant defensin (PDF) family	
At1g22900		**1.7**		Disease resistance-responsive (dirigent-like protein)/molecular function unknown	
At2g15120		4.9		Pseudogene, *disease-resistance* family protein/fatty acid elongase-related	
At5g17540		–1.7		HXXXD-type acyl-transferase family protein	
At5g54220		–1.4	1.7	Defensin-like (DEFL) family protein	
At1g21850		–1.7		sks8, copper ion-binding oxidoreductase	Cu
At1g30760		–1.5		FAD-binding domain-containing protein	
At1g13110		1.3		CYP71B7, cytochrome P450 family monooxygenase	Fe–haem
At2g12190		1.5		Cytochrome P450 family monooxygenase	Fe–haem
At5g14130		–1.9		Peroxidase, putative	Fe–haem
At5g38900		1.8		DSBA oxidoreductase family protein/thioredoxin superfamily	
At2g28710	DNA/RNA processes	2.0		Zinc finger (C2H2 type) family protein	Zn
At4g32980		1.7		ATH1, homeobox transcription factor	
At5g26630		–1.5		AGL35, transcription factor/MADS-box protein	
At1g09700		–1.3		HYL1, DRB1, double-stranded RNA binding/miRNA binding	
At5g20850		1.6		RAD51, DNA-dependent ATPase	
At5g46590		1.4		anac096, transcription factor/NAC domain-containing protein 96	
At5g38870		–1.5		Transposable element gene	
At5g66280	Cell wall modification	–1.6		GMD1, GDP-mannose 4,6-dehydratase	
At5g60490		–1.6		FLA12, fasciclin-like arabinogalactan protein/cell adhesion fasciclin domain	
At1g26240		1.4		Proline-rich extensin-like family protein	
At2g45110		–1.5		EXPB4, expansin family protein	
At5g39270		–2.3		EXPA22, expansin family protein	
At1g11590		–1.7		Pectin methylesterase, putative	
At4g03930		–1.7	1.7	Enzyme inhibitor/pectinesterase	

Table 2. Continued.

AGI code		*atfer1-3-4*++ versus WT++	WT++ versus WT	Name, function/domains	Metal binding
At3g20470		**–1.7**		GRP5, gylcine-rich protein 5/structural constituent of cell wall	
At3g28550		**1.6**	–1.6	Proline-rich extensin-like family protein	
At4g22870	Secondary metabolism	**–1.7**	1.7	LDOX, ANS, leucoanthocyanidin dioxygenase/anthocyanidin synthase, 2-oxoglutarate and Fe(II)-dependent oxygenase	Fe
At1g61720		–2.4		BAN, oxidoreductase	
At5g42800		–1.8		DFR, dihydrokaempferol 4-reductase	
At1g19830	Hormone metabolism	–1.5	1.6	SAUR-like auxin-responsive protein, putative	
At2g46530		–1.5		ARF11, transcription factor auxin response	
At1g63030		–1.4		ddf2, ethylene-responsive transcription factor/dwarf and delayed flowering/AP2-domain	
At5g52020		**–1.8**	1.6	AP2-domain (apetala), ethylene-responsive transcription factor	
At5g38970		–1.6		BR6OX1, brassinosteroid-6-oxidase1 / monooxygenase cytochrome P450 family	Fe–haem
At2g03760		1.3		ST1, brassinosteroid sulfotransferase	
At1g54450	Signalling	–1.3		Calcium-binding EF-hand family protein	Ca
At2g16250		**–1.9**		Leucine-rich repeat transmembrane protein kinase, putative	
At2g37330	Transport	1.4		*ALS3*, ABC transporter-like permease protein, required for Al-tolerance	
At1g53270		**–1.5**		ABCG10, ABC transporter family protein	
At3g59030		–1.9		*DTX41*, TT12 (transparent testa), putative vacuolar flavonoid/H^+ antiporter	
At5g04770		1.3		*CAT6*, cationic/basic amino acid transmembrane transporter	
At1g30690		–1.4		SEC14, cytosolic factor family protein/phosphoglyceride transfer family	
At1g08430		1.5		ALMT1, aluminium-activated malate transporter	
At4g17260	Others	–1.4		L-Lactate dehydrogenase, putative	
At4g15480		–1.5		GT84A1, UDP-glycosyltransferase/sinapate 1-glucosyltransferase	
At5g45700		–1.6		Haloacid dehalogenase-like hydrolase (HAD) superfamily/phosphatase	
At2g12050		1.4	–1.6	Pseudogene, similar to aintegumenta-like protein	
At1g64560		**–2.2**		Pseudogene of *S*-adenosylmethionine-dependent rRNA methyltransferase	
At5g40830		–1.2		Methyltransferase	
At2g24170	Unknown function	–1.3	1.5	EMP3, TMN10, putative TM9-type membrane protein of unknown function	
At1g68450		**1.6**		VQ motif-containing protein	
At2g22880		–1.4		VQ motif-containing protein	
At3g05460		–2.0		Sporozoite surface protein-related	
At5g12060		**–1.6**		Self-incompatibility protein-related	
At2g05540		1.7		Glycine-rich protein	
At2g05580		**–1.7**		Molecular function unknown	
At3g02670		**–2.0**		Proline-rich family protein	
At1g15840		–1.5		Molecular function unknown	
At1g65490		2.0		Molecular function unknown	
At3g02640		**–1.6**		Molecular function unknown	
At3g14060		1.8		Molecular function unknown	
At3g21190		–1.2		Molecular function unknown	
At4g09990		–1.5		Molecular function unknown	
At5g36710		–1.5		Molecular function unknown	

Table 3. Genes significantly regulated only in the atfer*1-3-4*++ versus WT comparison. The 43 genes which are differentially expressed only in the *atfer1-3-4*++ versus WT comparison (see Fig. 1A) are classified into functional categories. The fold change of transcript content is given. Bold characters in fold changes indicate adjusted *P*-values <0.05; those not in bold indicate $0.05 < P < 0.1$. The AGI codes, names, annotated functions, and/or domains, as well as metal binding of the corresponding proteins are listed. The columns WT++ versus WT and *atfer1-3-4* ++ versus *atfer1-3-4* indicate regulation of genes in response to Fe excess in wild-type and mutant flowers, respectively (Fig. 1B). Genes that were also regulated in flowers of PIC1 overexpressors (Duy *et al.*, 2011) are highlighted by a grey background; those that were re-analysed by qRT–PCR (Supplementary Table S1 at *JXB* online) are underlined.

AGI code		*atfer1-3-4* ++ versus WT	WT++ versus WT	*atfer1-3-4* ++ versus *atfer1-3-4*	Name, function/domains	Metal binding
At3g03910	Amino acid metabolism	–2.1	–2.0		*GDH3*, glutamate dehydrogenase 3	
AtCg01040	Protein metabolism+ modification	**3.8**			YCF5, protein complex assembly/cytochrome *c* complex assembly	
At2g47180	Carbohydrate metabolism	–1.6		–1.6	GolS1, galactinol synthase1 raffinose family/glycosyl group transferase	
AtCg00500	Lipid metabolism	**7.9**			*ACCD*, carboxytransferase beta subunit of acetyl-CoA carboxylase (ACCase) complex in plastids	
At5g33370		1.4			GDSL-motif lipase/hydrolase family protein	
At1g09080	Stress+redox	**–2.2**	–1.9	**–2.6**	BIP3, ATP binding/heat shock protein 70 site/protein folding, response to heat, pollen tube growth	
At4g36040		–1.3	–1.5	–1.5	DNAJ heat shock N-terminal domain-containing protein	
At2g47880		–2.0			Glutaredoxin family protein	
At5g64110		1.8			Peroxidase, putative	
At2g14560		–3.1			LURP1, up-regulated in response to *Hyaloperonospora parasitica*	
At3g27060	DNA/RNA processes	1.6			TSO2, oxidoreductase/ribonucleoside-diphosphate reductase	Fe
At3g27220		–1.5			MYB domain transcription factor/kelch repeat-containing protein	
At1g71030		–1.5		–1.8	MYBL2, MYB-related transcription factor	
At5g58900		**–1.5**		–1.5	MYB-related transcription factor	
At5g24470		–2.0			APRR5, transcription factor/two-component response regulator	
At1g78600		–1.6			LZF1, transcription factor/constans-like zinc finger family	Zn
At5g35970		–1.6			DNA-binding protein, putative	
At3g14530	Secondary metabolism	1.4	1.6		Geranylgeranyl pyrophosphate synthase/isoprenoids, non-mevalonate pathway	
At2g21220	Hormone metabolism	1.4	1.6		SAUR-like auxin-responsive protein family/ calmodulin binding	
At5g20820		**–1.8**			SAUR-like auxin-responsive protein family	
At3g23150		**–1.7**			ETR2, ethylene binding/histidine kinase receptor	
At4g17490		–1.9		–2.1	ERF6, ethylene-responsive transcription factor	
At5g61600		–1.7			ERF104, ethylene-responsive element-binding family/transcription factor	
At1g13260		–2.0			RAV1, AP2/B3-domain (apetala), ethylene-responsive transcription factor	
At5g39020	Signalling	**–1.6**	–1.4	–1.4	RLK1, receptor kinase family protein	
At1g73805		–2.0			Calmodulin binding	Ca

Table 3. Continued.

AGI code		*atfer1-3-4* ++ versus WT	WT++ versus WT	*atfer1-3-4* ++ versus *atfer1-3-4*	Name, function/domains	Metal binding
At2g03530	Transport	–1.3		–1.4	UPS2, ureide permease/uracil transport	
At1g27940		2.2			ABCB13/MDR15/PGP13, full-type ABC transporter protein	
At3g43790		–1.5			ZIFL2, Zn-induced major facilitator protein/sugar: hydrogen symporter	
At2g04050		**2.2**			DTX3, MATE efflux family protein	
At4g35770	Others	–1.6	–1.8		SEN1, senescence-associated protein	
At2g27080	Unknown function	1.7	2.0		Late embryogenesis abundant (LEA) hydroxyproline-rich glycoprotein family	
At2g30600		–1.5		–1.6	BTB/POZ domain-containing protein	
At1g13340		2.1			Molecular function unknown	
At1g20070		**–1.6**	–1.4	–1.5	Molecular function unknown	
At1g76240		**–2.2**	–1.5	–1.6	Molecular function unknown	
At2g20670		–1.5	–1.5		Molecular function unknown	
At3g01860		**–1.5**			Molecular function unknown	
At3g22240		**–1.5**			Molecular function unknown	
At4g35720		1.6			Molecular function unknown	
At5g05300		–1.3		–1.5	Molecular function unknown	
At5g57760		**–1.9**			Molecular function unknown	
At5g59080		**–1.8**			Molecular function unknown	

15 min), and centrifuged for 5 min at 18 000 rpm at 4 °C. The supernatant was discarded and the pellet was resuspended in 1.5 ml of 0.07% β-mercaptoethanol in acetone, vortexed, incubated for 5 min in an ultrasonic bath, vortexed again, cooled with liquid N_2, incubated for 30 min at –20 °C, and centrifuged for 5 min at 18 000 rpm at 4 °C. The supernatant was discarded and the pellet was dried in a SpeedVac for 10 min and stored at –20 °C until analysis.

Pellets were solubilized in 250 µl of sample rehydration buffer containing 8 M urea, 2% (w/v) CHAPS, 50 mM dithiothreitol (DTT), 2 mM phenylmethylsulphonyl fluoride (PMSF), and 0.2% (v/v) IPG buffer pH 3–10 (GE Healthcare, Uppsala, Sweden), stirred at 1000 rpm for 3 h at 38 °C in a Thermomixer Comfort device (Eppendorf AG, Hamburg, Germany), centrifuged at 10 000 *g* for 15 min at room tempertare, and filtered with 0.45 µm ultrafree-MC filters (Millipore, Bedford, MA, USA). Protein concentration was quantified immediately after extraction using Bradford's method with bovine serum albumin (BSA) as standard (Sigma).

In the proteomic and metabolomic analysis, a given genotype per treatment combination will be referred to hereafter as a class.

Two-dimensional electrophoresis (2-DE) analysis

Protein profiles were obtained using five independent biological replicates per treatment. The first dimension immunoelectric focusing (IEF) separation was carried out on 7 cm ReadyStrip IPG Strips (BioRad) with a 4–7 linear pH gradient in a Protean IEF Cell (BioRad), and the second dimension SDS–PAGE in 8 × 10 × 0.1 cm gels, as described in detail elsewhere (Rodriguez-Celma *et al.*, 2011). Gels were subsequently stained with Coomassie blue G-250 (Serva, Barcelona, Spain). 2-DE gel image analysis was carried out as described in Rodriguez-Celma *et al.* (2013). Briefly, stained gels were scanned, and experimental M_r and pI values calculated by mobility comparisons with standard markers. Spot detection, gel matching, and analysis were performed with PDQuest 8.0 software (BioRad). Missing spot volumes were estimated using a sequential K-Nearest Neighbor algorithm. Consistent spots were those present in at least 80% of the replicates from at least one class. Differentially expressed spots were defined using a Student's *t*-test value of $P < 0.10$. Protein response ratios were defined as the abundance in a given class divided by the abundance in the control class; when ratios were <1, the inverse was taken and the sign changed. Only proteins with mean response ratios >2.0 or below –2.0 were considered relevant and analysed further. Partial least square (PLS) analysis was applied to the identified protein species using SPSS v. 15 (SPSS Inc., Chicago, IL, USA).

Protein in-gel digestion and identification by nano-high performance liquid chromatography–tandem mass spectrometry

Selected spots were excised, in-gel digested with trypsin, and analysed by nano-HPLC–tandem mass spectrometry as described in detail in Rodriguez-Celma *et al.* (2013). Protein identification was performed by searching in the non-redundant NCBI 20120324 (17 612 906 sequences; 6 046 335 507 residues) and Plants_EST EST_111 (155 120 040 sequences; 27 373 983 152 residues) databases using the Mascot search engine (Matrix Science, London, UK). The search parameters were: monoisotopic mass accuracy, peptide mass tolerance ±0.2 Da, fragment mass tolerance ±0.6 Da, one allowed missed cleavage, allowed fixed modification carbamidomethylation (Cys), and variable modification oxidation (Met). Positive identification was assigned with Mascot scores above the threshold level ($P < 0.05$), at least two identified peptides with a score above homology, 10% sequence coverage, and similar experimental and theoretical molecular weight and pI. The GO biological process annotation (http://www.geneontology.org) of the individual identified proteins was used for classification.

Metabolite analysis and data processing

Metabolite profiles were obtained using six independent biological replicates per treatment. Metabolite extraction was carried out as previously described for leaf extracts (Fiehn and Weckwerth, 2003; Fiehn *et al.*, 2008; Rellán-Álvarez *et al.*, 2011). Dried extracts were derivatized as described elsewhere (Fiehn *et al.*, 2008). Derivatized samples (1 µl) were injected randomly in split-less mode with a cold injection system (Gerstel, Mülheim an der Ruhr, Germany) and separated in a GC device (Agilent 6890, San Jose, CA, USA) using an integrated guard column (Restek, Bellefonte, PA, USA) and an Rtx 5Sil MS column (30 m×0.25 mm, 0.25 µm film thickness). The GC device was connected to a Leco Pegasus IV time-of-flight mass spectrometer (TOFMS) controlled with Leco ChromaTOF software v.2.32 (Leco, St. Joseph, MI, USA). Peak detection and mass spectra deconvolution were performed with Leco Chroma-TOF software v.2.25, and GC-MS chromatograms were processed as described previously (Fiehn *et al.*, 2008).

Metabolite data were normalized using the sample fresh weight and the sum of all metabolite peak heights in a single run, to account for small GC injection variations. The resulting data were multiplied by a constant factor in order to obtain values without decimal figures. Peaks were identified using the Fiehn Lib database (http://fiehnlab.ucdavis.edu/projects/FiehnLib/index_html). Metabolite spectra, including those of identified metabolites and unknowns, can be queried and downloaded at the Fe Chlorosis Database (fechlodb.fiehnlab.ucdavis.edu). Data were analysed to check for possible correlations between peak height values and peak variance, and since a positive correlation was found a $\log_{10}$ transformation of the data was carried out to avoid variance-mean dependence (Chich *et al.*, 2007).

Statistical analysis of the normalized data was carried out with Statistica software (v.9.0. StatSoft, Inc., Tulsa, OK, USA). Only those metabolites present in at least 80% of the samples from at least one class were considered. Significant changes in metabolite levels were detected for each class using one-factor analysis of variance (ANOVA; $P \leq 0.05$). Metabolite response ratios were defined as the level in the class divided by the level in the control class; when ratios were <1, the inverse was taken and the sign changed. Only metabolites with mean response ratios (using the non-$\log_{10}$ transformed data) >1.5 or below –1.5 were considered relevant and are discussed in this study. Multivariate analysis (supervised PLS) was used to study the clustering of the samples, as well as to find out which metabolites were responsible for the separation between classes.

For all the metabolomic profiling analyses, the recommended guidelines provided by Fiehn *et al.* (2008) were followed. Full documentation of metabolite profiling data acquisition and interpretation, according to Fernie *et al.* (2011), is also disclosed in Supplementary Table S2 at *JXB* online.

Hormone analysis

The concentration of the main plant hormones in the flower samples of WT and *atfer1-3-4 Arabidopsis* plants was determined using HPLC–electrospray–mass spectrometry (HPLC-ESI-MS/MS) as described below.

The following hormones were analysed and quantified: indole-3-acetic acid (IAA), ABA, *trans*-zeatin (Z), *trans*- and *cis*-zeatin riboside (t-ZR and c-ZR), dihydrozeatin riboside (DHZR), and isopentenyladenosine (iPR).

The extraction and purification of IAA and ABA were carried out using the method described in detail by Bacaicoa *et al.* (2011), using 250 mg of frozen flowers and 4 ml of extraction medium. Overnight extraction, centrifugation, re-extraction, and purification of the extract were done as in Bacaicoa *et al.* (2011). Before the injection in the HPLC-ESI-MS/MS system, the solution was centrifuged at 12 000 *g* for 5 min. IAA and ABA were determined by HPLC-ESI-MS/MS using multiple reaction monitoring (MRM) in the negative-ion mode, employing multilevel calibration curves with deuterated hormones as internal standards, as indicated in Bacaicoa *et al.* (2011). Compound-dependent parameters are listed in Supplementary Table S3 at *JXB* online. The extraction and purification of cytokinins were carried out using the method described by Dobrev and Kamínek (2002), with some modifications: 250 mg of frozen flower tissue were ground in a mortar with liquid N_2 and homogenized with 4 ml of pre-cooled (–20 ºC) methanol:water:formic acid (15:4:1, v/v/v). Deuterium-labelled cytokinin internal standards ($[^2H_5]$Z, $[^2H_5]$tZR, $[^2H_6]$iP, $[^2H_6]$iPR, $[^2H_7]$ BA, $[^2H_7]$BAR, and $[^{13}C_5]$oT; all from Olchemim Ltd, Olomouc, Czech Republic), were added (40 µl of a stock solution of 50 ng ml^{-1} of each standard in methanol) to the extraction medium. Extraction was then performed according to Bacaicoa *et al.* (2011) until reaching the aqueous phase after evaporation at 40 ºC. Then, 2 ml of 1 M formic acid was added, and applied to an Oasis MCX column (3 cm^3, 60 mg) (Waters Co., Milford, MA, USA; Ref. 186000254), pre-conditioned with 4 ml of methanol and 2 ml of 1 M formic acid. The column was washed successively with 2 ml of 1 M formic acid, 2 ml of methanol, and 2 ml of 0.35 M NH_4OH, and the cytokinin bases, ribosides, and glucosides were eluted with 2 ml of 0.35 M NH_4OH in 60% (v/v) methanol. This eluted fraction was evaporated to dryness in a vortex evaporator and re-dissolved in 250 µl of methanol:0.05% formic acid (40:60, v/v). Before the injection in the HPLC-ESI-MS/MS system, the solution was centrifuged at 12 000 *g* for 5 min. Cytokinins were quantified by HPLC-ESI-MS/MS as in Bacaicoa *et al.* (2011), but with a different reverse-phase column (Tracer Excel 120 ODSA 3 µm, 100 × 4.6 mm; Teknokroma, Barcelona, Spain). A linear gradient of methanol (A) and 0.05% formic acid in water (B) was used: 35% to 95% A in 11 min, 95% A for 3 min, and 95% to 35% A in 1 min, followed by a stabilization time of 5 min. The flow rate was 0.25 ml min^{-1}, the injection volume was 40 µl, and column and sample temperatures were 30 °C and 20 ºC, respectively. The detection and quantification of cytokinins were carried out using multiple MRM in the positive-ion mode, employing multilevel calibration curves with deuterated cytokinins as internal standards. Compound-dependent parameters are listed in Supplementary Table S4 at *JXB* online. The source parameters were: curtain gas, 172.37 kPa; GS1, 344.74 kPa; GS2, 413.69 kPa; ion spray voltage, 5000 V; and temperature, 600 ºC. Data samples were processed using Analyst 1.4.2 Software from AB SCIEX (Framingham, MA, USA).

Results

Comparison of the flower transcriptomes of Col-0 and atfer1-3-4 Arabidopsis *plants grown under iron-sufficient or excess conditions*

Differential gene expression in flowers of the triple ferritin mutant *atfer1-3-4* (Ravet *et al.*, 2009*a*) and Col-0 WT plants, grown in Fe-sufficient control conditions or under excess Fe (*atfer1-3-4*++ and WT++, respectively), was monitored by microarray analysis. The differential regulation observed was low, with a total of 276 genes significantly regulated (Fig. 1A; Supplementary Table S5 at *JXB* online). Most fold changes ranged between 1.4 and 3.5, and only a few showed strong alterations (7). All ferritin genes mutated in *atfer1-3-4* (Ravet *et al.*, 2009*a*) were down-regulated when compared with the WT, with strong effects for the knockouts of *AtFER1* and *AtFER4* and a mild decrease for the knockdown of *AtFER3* (Fig. 1C), the latter only being significant when the *atfer1-3-4* mutant was challenged with excess Fe (see number 3 in Supplementary Table S5). When flower transcript levels in mutants versus the WT in all three possible combinations were compared, 121 (*atfer1-3-4* versus WT), 187 (*atfer1-3-4*++ versus WT++), and 146 (*atfer1-3-4*++ versus WT) genes were found to be significantly regulated (adjusted *P*-value ≤0.10;

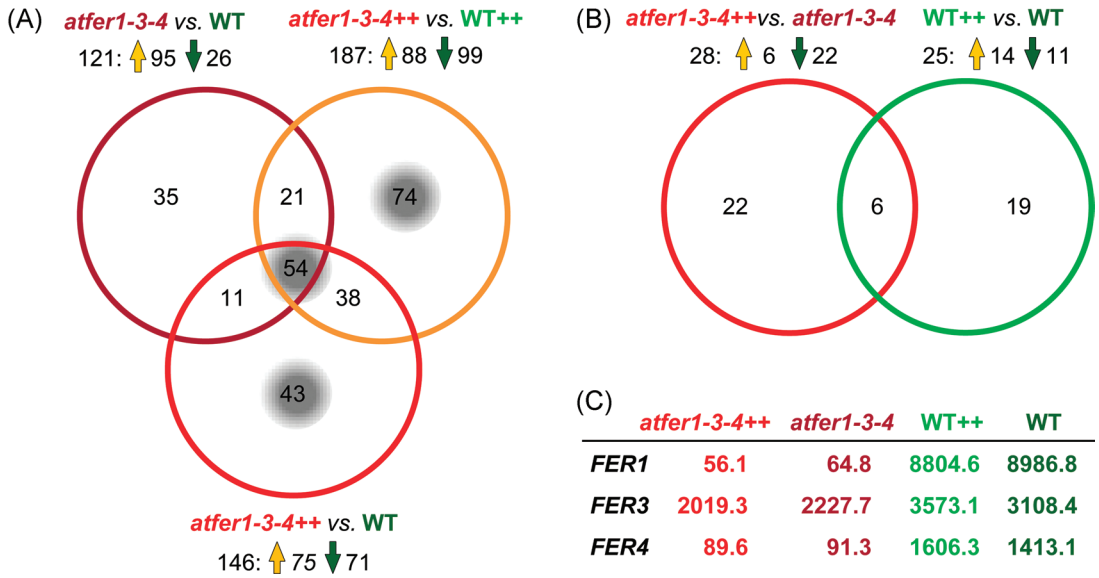

(C)

	atfer1-3-4++	atfer1-3-4	WT++	WT
FER1	56.1	64.8	8804.6	8986.8
FER3	2019.3	2227.7	3573.1	3108.4
FER4	89.6	91.3	1606.3	1413.1

Fig. 1. Changes in *Arabidopsis* flower transcripts of *atfer1-3-4* mutants and the wild type. Overlapping regulation is shown by Venn diagrams. Numbers of regulated genes are given; up- and down-regulation is indicated by orange and green arrows, respectively (for fold changes see Supplementary Table S5 at JXB online). (A) Differentially expressed genes (*P*-value ≤0.1) in flowers of *atfer1-3-4* mutants compared with the Col-0 wild type (WT) under Fe-sufficient and Fe excess (++) conditions. In total, 276 genes were significantly regulated when comparing *atfer1-3-4* versus WT, *atfer1-3-4++* versus WT++, and *atfer1-3-4++* versus WT. Gene groups of interest discussed in the text are highlighted by a grey background. (B) Transcript changes (*P*-value ≤0.2) induced by Fe excess (++) in *atfer1-3-4* and the wild type using the respective Fe-sufficient conditions as control. Note that all genes regulated in *atfer1-3-4++* versus *atfer1-3-4* and WT++ versus WT are also differentially expressed in one of the comparisons depicted in (A). (C) Mean signal values (arbitrary units) of mRNA from mutated ferritin genes (*AtFER1*, *AtFER3*, and *AtFER4*) in flowers of all samples analysed.

Fig. 1A). Interestingly, in control conditions, the majority of genes (95 of 121) in *atfer1-3-4* were up-regulated, whereas upon Fe excess, the increase and decrease of transcript numbers was more evenly distributed, when compared both with WT++ (88 up and 99 down) and with WT (75 up and 71 down). When compared with transcript regulation in flowers overexpressing the chloroplast Fe permease PIC1 (PIC1ox; Duy *et al.*, 2011), a high number of overlapping genes was found (63 out of 276, 23%; see highlighted genes in Tables 1–3 and Supplementary Table S5). In comparison with mutant versus WT changes, regulation in response to Fe was less pronounced and less significant (adjusted *P*-value ≤0.20), with only 28 (*atfer1-3-4++* versus *atfer1-3-4*) and 25 (WT++ versus WT) genes showing differences (Fig. 1B). Iron excess in flowers of the *atfer1-3-4* mutant mainly induced down-regulation of genes (22 of 28), while in the WT the increases and decreases in transcript numbers were evenly distributed (14 up and 11 down). To correlate data output from transcriptomics, proteomics, and metabolomics throughout the entire study, the following 17 functional categories were chosen for sorting of differentially expressed genes and proteins (see Tables 1–4 and Supplementary Table S5): metal (iron) homeostasis and binding, amino acid metabolism, protein metabolism and modification, carbohydrate metabolism, photosynthesis, cofactor biosynthesis, lipid metabolism, stress and redox, DNA/RNA processes, cell cycle and cell biogenesis, cell wall modification, secondary metabolism, hormone metabolism, other processes, signalling, transport, and unknown function. For all putative functional annotations cited in the following sections: (i) the MAPMAN *Arabidopsis* pathway analysis program (Thimm *et al.*, 2004); (ii) TAIR (The Arabidopsis Information Resource, TAIR Gene Model on www.arabidopsis.org, 16 June 2012); and (iii) the ARAMEMNON database (aramemnon.botanik.uni-koeln.de; Schwacke *et al.*, 2003) were referred to.

The focus was first on overlaps in mutant versus WT samples in all three comparisons (*atfer1-3-4* versus WT, *atfer1-3-4++* versus WT++, and *atfer1-3-4++* versus WT). This overlap contained 54 differentially expressed genes (44 with *P*-value <0.05), which reflects the influence of the ferritin null mutant background regardless of the Fe status of the plants (Fig. 1A). Disposition of these genes into functional categories (Table 1) revealed that the biggest focus of transcript regulation was on stress- and redox-related functions, accounting for 28% of the total changes. In this category, all genes were up-regulated in *atfer1-3-4*, and most of them (7 out of 15) were Fe–haem-binding oxidoreductases. Further, besides the *AtFER1* and *AtFER4* genes, the largest fold changes (>10.0) were also found in this category: an FAD-binding berberine family protein (At1g26390), and, when plants were challenged with excess Fe, a P450 monooxygenase (At4g31970). In addition to stress and redox, transcriptional regulation and hormone metabolism were additional targets for gene regulation (i.e. more than three genes differentially expressed). In general, hormone-related genes were up-regulated, whereas the transcriptional regulation category contained genes up- and down-regulated. For only three genes, Fe excess treatment in the comparisons *atfer1-3-4++* versus WT and *atfer1-3-4++*

versus WT++ induced a reciprocal regulation (i.e. transcript decrease) when compared with Fe-sufficient conditions in *atfer1-3-4* versus WT (increase of transcript content; Table 1): *TCH4* (At5g57560), a xyloglucan endotransglycosylase involved in cell wall modification; At4g27280, a Ca-binding EF hand family protein; and At4g36500, a protein of unknown function predicted to be localized in mitochondria and regulated in response to various stresses or auxin (TAIR annotation). The largest overlap with gene regulation in flowers overexpressing the chloroplast Fe permease PIC1 (PIC1ox; Duy *et al.*, 2011) was for genes involved in hormone metabolism. To map the effect of excess Fe on the mutant versus WT regulation, those genes that were differentially expressed in the *atfer1-3-4*++ versus WT++ comparison were selected (74 genes, 14 with a *P*-value <0.05; Fig. 1A, Table 2). In addition to the functional categories described above, protein metabolism and modification, cell wall modification, and transport were also extra targets for gene regulation. Metal homeostasis-associated genes were represented by the ferric reductase oxidase FRO3 (At1g23020), induced by Fe deficiency, and involved in Fe transport processes in the root vascular cylinder (Mukherjee *et al.*, 2006), which was increased in the mutant when compared with the WT. Overall, genes related to protein and hormone metabolism were down-regulated, while those belonging to stress and redox processes, in contrast to those listed in Table 1 (overlaps of all mutant–WT comparisons), were now evenly distributed among increases and decreases. With regard to the new targets, protein metabolism and cell wall modification showed a general down-regulation, whereas transport-related genes were evenly distributed (three up- and three down-regulated). Among the transporters increased in *atfer1-3-4*++ when compared with WT++, two related to Al tolerance were found: the phloem-localized ABC transporter permease-like protein ALS3 (At2g37330) (Larsen *et al.*, 2005) and ALMT1 (At1g08430), an Al-activated malate transporter (Liu *et al.*, 2009, 2012). The other up-regulated gene was CAT6 (At5g04770), a putative cationic amino acid transporter. Down-regulated transporter genes were: the ABC-transporter ABCG10 (At1g53270); DTX41 (At3g59030), a putative vacuolar flavonoid/H+ antiporter of the MATE family; and a Sec14p-like phosphatidylinositol transfer family protein (At1g30690) with potential α-tocopherol transport function. The 43 genes differentially expressed only in *atfer1-3-4*++ versus WT (14 with a *P*-value <0.05; Fig. 1A, Table 3) should mainly reflect the effect of Fe excess on the mutant only. The targets for gene regulation within this comparison were again stress and redox, DNA/RNA processes, and hormone metabolism, and in general showed a down-regulation. However, the largest change was an up-regulation (8-fold increase) of ACCD (AtCg00500), the plastid-encoded carboxytransferase β-subunit of the acetyl-CoA carboxylase complex. This complex catalyses the carboxylation of acetyl-CoA to produce malonyl-CoA, the first committed step in fatty acid synthesis. Chloroplast-encoded genes appeared to be predominantly up-regulated in the *atfer1-3-4*++ versus WT comparison. Besides ACCD, YCF5, which is involved in the assembly of the cytochrome *c* complex (AtCg01040, Table 3, 4-fold increase), and RPS16, a plastid-localized S16 ribosomal protein (AtCg00050, Table 1, 14-fold increase) were also found to be strongly induced in *atfer1-3-4*++ versus WT. This suggests that under excess Fe the loss of ferritin function affects chloroplast gene expression and in consequence metabolism.

Comparison of the flower proteomes of Col-0 and atfer1-3-4 Arabidopsis *plants grown under iron-sufficient or excess conditions*

Typical real scans of 2-DE gels obtained from protein extracts of flowers from Col-0 and triple ferritin mutant grown in control conditions or under Fe excess (WT, WT++, *atfer1-3-4*, and *atfer1-3-4*++, respectively) are shown in Fig. 2A–D. The average number of detected spots (mean ±SD; n=5) was 362 ± 35, 328 ± 39, 341 ± 25, and 350 ± 40 in WT, WT++, *atfer1-3-4*, and *atfer1-3-4*++, respectively (Supplementary Table S6 at *JXB* online). The total number of consistent spots was 377. A composite averaged virtual map containing all spots present in all classes is shown in Fig. 2E.

A first comparison was made taking the WT protein profile as control. Approximately 3% (11), 6% (20), and 6% (21) of the spots in the WT++, *atfer1-3-4*, and *atfer1-3-4*++ classes, respectively, showed significant relative abundance changes (spots are highlighted in Fig. 2F–H; Supplementary Table S6 at *JXB* online). When a second comparison was carried out with the same criteria between *atfer1-3-4*++ and *atfer1-3-4*, 6% (22) of the spots showed changes (Fig. 3A; Supplementary Table S6). A third comparison between *atfer1-3-4*++ and WT++ revealed that 3% (12) of the spots showed changes (Fig. 3B; Supplementary Table S6). The total number of spots having consistent changes between classes was 63, and 98% of them (62) were unambiguously identified by MS (Table 4; Supplementary Fig. S1A–E). The PLS analysis showed a good separation between treatments WT and *atfer1-3-4* ++, whereas WT++ and *atfer1-3-4* clustered together and apart from the other two (Supplementary Fig. S2A).

The Fe excess treatment in WT plants only caused decreases in the relative signal intensity of 11 spots (green symbols in Fig. 2F) and all of them were identified (Table 4; Supplementary Fig. S1A at *JXB* online). Proteins belonged to different metabolic pathways, including amino acid and protein metabolism (spots 3, 6, and 13), carbohydrate metabolism (spot 25), photosynthesis (spot 28), cofactor biosynthesis (spot 34), stress-related processes (spots 39 and 40), DNA replication (spot 43), and N metabolism (spot 53). Spot 56 was an uncharacterized protein. The largest fold decreases in this comparison were found for an elongation factor involved in protein translation (25-fold; spot 13) and for a β-ureidoropionase (10-fold; spot 53), a hydrolase acting in pyrimidine catabolism that yields β-alanine, CO_2, and NH_3.

When comparing the averaged map of flowers from *atfer1-3-4* versus WT, two spots increased in signal intensity (orange symbols in Fig. 2G). They were identified as the large subunit of Rubisco and an uncharacterized protein (spot 27 and spot 58, respectively, in Table 4 and Supplementary Fig. S1B at *JXB* online). Seventeen spots decreased, whereas one more (spot 50) was no longer detected (green and blue symbols,

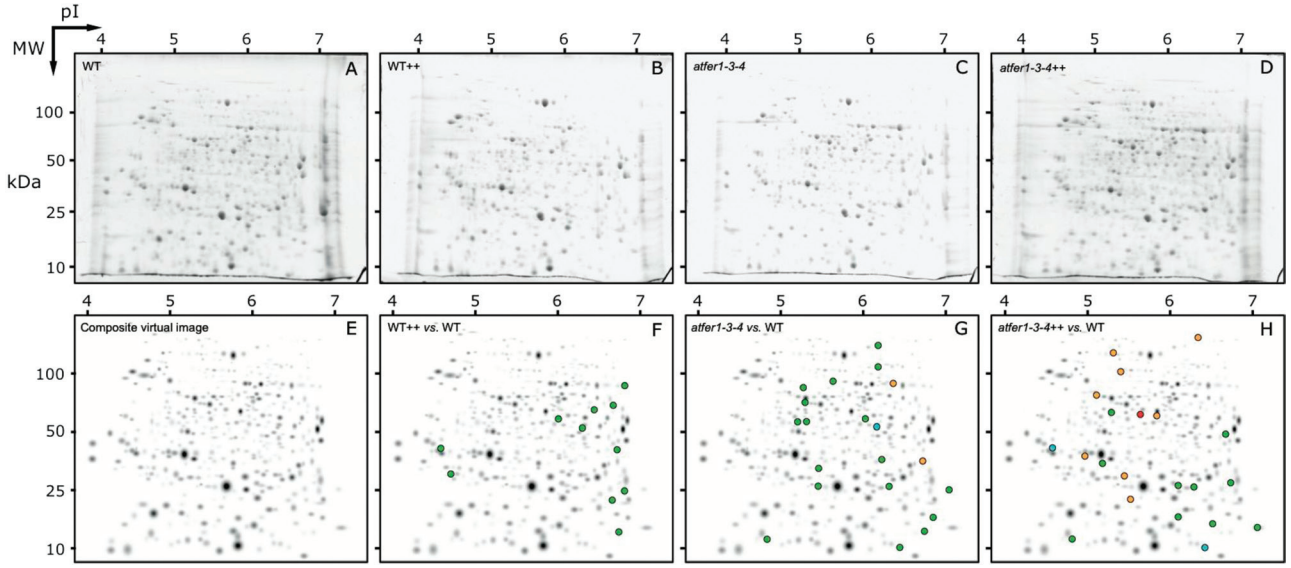

Fig. 2. 2-DE IEF–SDS PAGE protein profile maps of whole flower extracts from *Arabidopsis thaliana* plants, and changes in spot abundance taking the WT as control. Proteins were separated in the first dimension in linear IPG pH 4–7 gel strips and in the second dimension in 12% acrylamide vertical gels. Scans of typical gels of flower extracts from WT, WT++, *atfer1-3-4*, and *atfer1-3-4*++ plants are shown in A, B, C, and D, respectively. To facilitate visualization of the studied spots, a virtual composite image (E) was created containing all spots present in the real gels A, B, C, and D. F, G, and H show spots whose relative abundance changed in WT++, *atfer1-3-4*, and *atfer1-3-4*++ when compared with the WT. Spots that decreased in abundance or were no longer detected when compared with control maps are marked with green and blue symbols, respectively, and those with increased abundance or newly detected spots are marked with orange and red symbols, respectively.

respectively, in Fig. 2G). All of them were identified (Table 4; Supplementary Fig. S1B) and assigned to amino acid (spots 4 and 5), carbohydrate (spots 22–24 and 26), and protein (spots 15 and 16) metabolic processes, cofactor biosynthesis (spot 34), lipid metabolism (spot 36), stress (spots 38 and 41), DNA- and RNA-related processes (spots 42–44), cell cycle (spot 47), and secondary metabolism (spot 50). Spot 59 was an uncharacterized protein. The largest decreases found were for the GSL lipase, an extracellular enzyme involved in lipid degradation (24-fold, spot 36), the monothiol glutaredoxin-S15 (15-fold, spot 38), a mitochondrial enzyme containing an Fe–S cluster involved in cell redox homeostasis, and a strictosidine synthase (no longer detected, spot 50), which is involved in indole alkaloid biosynthesis.

Comparison of *atfer1-3-4*++ versus WT showed eight spots that increased and one appearing *de novo* (orange and red symbols in Fig. 2H, respectively). All of them were identified (Table 4; Supplementary Fig. S1C at *JXB* online) and five were ascribed to amino acid and protein (spots 1, 10, and 11) and carbohydrate metabolism (spots 18 and 21). Spot 52 was in the Others category, and spots 57, 60, and 61 were uncharacterized proteins. Ten spots decreased (green symbols in Fig. 2H), and two were no longer detected (blue symbols in Fig. 2H). All of them were identified (Table 4; Supplementary Fig. S1C) and assigned to protein metabolism (spots 13, 14, and 17), photosynthesis (spots 29–31), lipid metabolism (spot 36), stress (spot 38), RNA-associated processes (spot 42), cell cycle (spot 46), and others (spots 54 and 55). The largest changes within this comparison were found for an elongation factor (spot 13), an RNA-binding protein related to the stress response (spot 42), which was no longer detected, and the cytosolic fructose-1,6-biphosphatase (spot 18), which was detected de novo.

In the *atfer1-3-4*++ versus *atfer1-3-4* comparison, 18 spots increased and two appeared *de novo* (orange and red symbols in Fig. 3A, respectively). Nineteen of them were identified (Table 4; Supplementary Fig. S1D at *JXB* online) and ascribed to amino acid (spots 1 and 5), protein (spots 7, 9 and 12), lipid (spot 35), carbohydrate (spots 18–20 and 26), and secondary (spot 50) metabolism, thiamine biosynthesis (spots 32 and 33), stress (spot 41), and cell cycle (spots 45 and 47). Spot 52 was in the Others category, and spots 61 and 62 were uncharacterized proteins. Spot 63 could not be identified. One spot, 49, was no longer detected and was identified as β-xylosidase 4, a protein assigned to cell wall modification (green and blue symbols in Fig. 3A; Table 4; Fig. S1D), and another spot, 56, decreased in relative intensity and was an uncharacterized protein. In addition to the proteasome subunit β-type-2-B (spot 7) and the strictosidine synthase (spot 50), which were detected *de novo*, the largest change in this comparison was an increase in a chloroplastic haloacid dehalogenase-like protein (21-fold, spot 62).

The *atfer1-3-4*++ versus WT++ comparison revealed 10 spots increasing in intensity, and one appearing *de novo* (orange and red symbols in Fig. 3B, respectively). All of these were identified (Table 4; Supplementary Fig. S1E at *JXB* online) and included in amino acid (spots 1–3), protein (spot 8), carbohydrate (spots 18 and 20), and secondary (spot 51) metabolism, stress (spot 40), and cell wall (spot 48) categories. Spot 52 was in the Others category, and spot 61 was

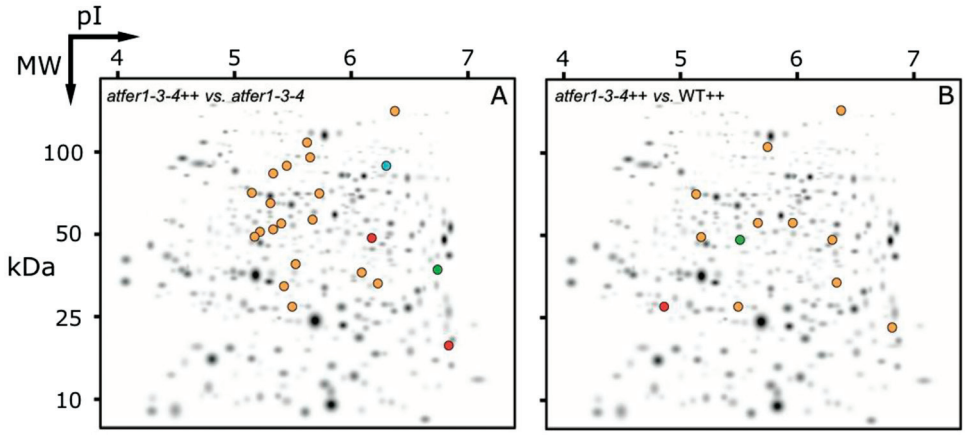

Fig. 3. Changes in spot abundance in the 2-DE IEF–SDS–PAGE protein profile maps of whole flower extracts from *atfer1-3-4*++, taking *atfer1-3-4* as the control. Spots that decreased or were no longer detected when compared with control maps are marked with green and blue symbols, respectively, and those with increased response ratios (i.e. abundance) or newly detected spots are marked with orange and red symbols, respectively.

an uncharacterized protein. One decreasing spot, identified as a GDSL esterase/lipase, was related to lipid metabolism (green symbol in Fig. 3B; spot 37 in Supplementary Fig. S1E). The largest changes within this comparison were a 100-fold increase in a cysteine protease (spot 8) and a 10-fold increase in a xyloglucan endotransglucosylase (spot 48) that participates in cell wall construction of growing tissues by modifying xyloglucan polymers, an essential constituent of the primary cell wall.

The information on the changes in protein abundance overlapping in the different classes was demonstrated using Venn diagrams, as for transcriptomic data analysis (Fig. 4). No protein overlap was found in the *atfer1-3-4* versus WT, *atfer1-3-4*++ versus WT++, and *atfer1-3-4*++ versus WT comparisons. The second group of interest, containing proteins changing only in the *atfer1-3-4*++ versus WT++ comparison (Fig. 4, Table 4), contained eight protein species, most of them (seven) showing increases in relative abundance, except for one (spot 37, identified as a GDSL esterase/lipase). The amino acid/protein metabolism category, which contained a D-3-phosphoglycerate dehydrogenase, an arginase, and a cysteine protease (spots 2, 3, and 8, respectively), was a target for regulation at the protein level. In agreement with the target categories found in the transcriptomic analysis for gene regulation, protein species in this group were related to stress and redox, including an Fe oxidoreductase (flavonol synthase, spot 51), a galactose oxidase (spot 20), and a glutathione *S*-transferase (spot 40), and to cell wall modification (xyloglucan endotransglucosylase, spot 48). Although the hormone category did not contain any protein species, at least three of the proteins in this second group (spots 40, 48, and 51) are auxin regulated (UniProt DB annotation). The third group of interest contained 14 protein species changing only in the *atfer1-3-4*++ versus WT comparison (Fig. 4, Table 4). This analysis revealed that protein metabolism (spots 10, 11, 13, 14, and 17) and photosynthesis [two spots for the cyt*b6f* protein (spots 29 and 30) and OEC23 (spot 31)] were target categories for regulation at the protein level.

Comparison of the flower metabolomes of Col-0 and atfer1-3-4 Arabidopsis *plants grown under iron-sufficient or excess conditions*

The metabolite profile of whole flower extracts from the *A. thaliana* triple ferritin mutant *atfer1-3-4* and the Col-0 WT, grown in control conditions and under excess Fe (*atfer1-3-4*++ and WT++, respectively), were studied using GC-MS. Only metabolites present in at least 80% of any sample class (in five out of six replicates) were taken into consideration. A total of 251 of such consistently present metabolites were detected, and 103 of them were identified using the Fiehn Lib database, whereas 148 were unknowns (a complete metabolite list is shown in Supplementary Table S7 at *JXB* online).

When comparing the metabolite profiles of the different sample classes with those of the WT, 10 identified metabolites showed significant changes (at $P \leq 0.05$) and mean response ratios >1.5 or below –1.5. One, three, and 10 of the known metabolites showed changes in the WT++, *atfer1-3-4*, and *atfer1-3-4*++ classes, respectively (Table 5). The largest increases in abundance were for urea (10-fold increase in *atfer1-3-4*++), 2-hydroxyglutaric and threonic acids (2- to 3-fold increases in *atfer1-3-4* and *atfer1-3-4*++), and gluconic acid lactone (2-fold increases in *atfer1-3-4*++). The largest decreases in abundance were for ascorbic acid (80% decreases in WT++ and *atfer1-3-4*++), and salicin (75% in *atfer1-3-4*++). On the other hand, significant changes were observed in a total of 25 unknown metabolites: three, seven, and 22 of them in the WT++, *atfer1-3-4*, and *atfer1-3-4*++ classes, respectively (Table 5). These unknowns accounted for 75, 70, and 69% of the total metabolites changing significantly in the WT++, *atfer1-3-4*, and *atfer1-3-4*++ classes, respectively, when compared with the WT.

The clustering of metabolites was studied in each sample class using PLS analysis, including both the identified and unknown metabolites (Supplementary Fig. S2B at *JXB* online). The WT, WT++, *atfer1-3-4* , and *atfer1-3-4* ++ classes separated in clusters. The first vector (v1) explained

Table 4. Proteins identified in two-dimensional IEF–SDS–PAGE. Positive identification was retained with Mascot scores (sco) above the threshold level ($P < 0.05$), at least two identified peptides with a score (pep/ion) above homology, 10% sequence coverage (%), and similar experimental (exp) and theoretical (th) molecular weight (MW) and pI. Relative spot intensity changes in the WT++ versus WT, *atfer1-3-4* versus WT, *atfer1-3-4* versus WT, *atfer1-3-4*++ versus *atfer1-3-4*, and *atfer1-3-4*++ versus WT++ comparisons are presented as fold (Student's *t*-test, $P < 0.1$; n=5). Bold and regular characters in fold changes indicate $P < 0.05$ and $0.05 < P < 0.1$, respectively. New and ND indicate spots that have been newly detected or no longer detected, and (–) denotes no significant change. Function was inferred from GO annotation. Spot number (as in Supplementary Fig. 1 at *JXB* online), UniProt. and AGI codes are shown in columns 1, 2, and 3.

n	UniProt	AGI code	WT++ versus WT	*atfer* versus WT	*atfer*++ versus WT	*atfer*++ versus *atfer*	*atfer*++ versus WT++	Protein name/function	Sco/pep/ion	%	MW/pI th	MW/pI exp	Metal binding
Amino acid metabolism													
1	O80988	At2g26080	–	–	**3.4**	**6.3**	**3.1**	Glycine dehydrogenase 1	454/9/9	11	114.7/6.2	111.4/6.2	
2	O04130	At1g17745	–	–	–	–	3.0	D-3-Phosphoglycerate-DH	625/12/8	17	66.8/5.8	71.3/5.7	
3	Q9ZPF5	At4g08870	**–3.3**	–	–	–	**3.6**	Putative arginase	834/36/18	48	38.1/5.9	35.4/6.2	Mn
4	F4I7I0	At1g17290	–	–2.4	–	–	–	Alanine aminotransferase	723/15/13	28	60.4/5.9	56.5/5.6	
5	P93832	At1g80560	–	–2.3	–	3.3	–	3-Isopropylmalate DH 2	607/14/12	28	43.5/5.8	44.3/5.3	Mn, Mg
6	Q9SWG0	At3g45300	–2.1	–	–	–	–	Isovaleryl-CoA-DH	817/22/15	33	45.4/7.5	41.5/6.3	
Protein metabolism/modification													
7	O24633	At4g14800	–	–	–	New	–	Proteasome subunit β type-2-B	72/2/2	14	22.1/6.2	19.2/6.6	
8	Q9LNC1	At1g06260	–	–	–	–	**100**	Cysteine proteinase-like protein	439/12/7	28	38.3/7.5	24.9/4.9	
9	C0Z361	At5g56500	–	–		6.6	–	cpn60 chaperonin family protein	873/16/14	32	63.7/5.7	65.1/5.6	
10	Q9LKR3	At5g28540	–	–	2.8	–	–	Heat shock 70 kDa protein 11	1670/55/30	48	73.9/5.1	81.9/5.3	
11	Q43349	At3g53460	–	–	2.6	–	–	29 kDa ribonucleoprotein	480/12/8	29	35.3/5.2	28.7/5.0	
12	Q9LDZ0	At5g09590	–	–	–	2.3	–	Heat shock 70 kDa protein 10	1608/46/28	46	73.2/5.6	73.9/5.5	
13	Q9SCX3	At5g19510	**–25.1**	–	**ND**	–	–	Elongation factor 1-β2	441/12/8	41	24.2/4.4	30.4/4.6	
14	O23727		–	–	**–4.6**	–	–	Peptidyl-prolyl *cis-trans* isomerase	680/20/12	58	24.9/5.1	27.2/5.2	
15	Q9LY14	At5g07470	–	–2.4	–	–	–	Peptide methionine sulphoxide reductase A3	148/5/5	21	22.8/5.3	26.2/5.4	
16	O65282	At5g20720	–	–2.1	–	–	–	Chaperonin 10	304/6/5	19	26.9/8.9	22.6/5.4	Cu
17	O23710	At3g27430	–	–	–2.0	–	–	Proteasome subunit β type-7-A	322/10/6	21	29.8/6.7	23.4/6.6	
Carbohydrate metabolism													
18	Q9MA79	At1g43670	–	–	**New**	4.7	4.7	Fructose-1,6-bisphosphatase	696/19/12	36	37.7/5.3	39.4/5.6	Mg
19	Q9C6Z3	At1g30120	–	–	–	**6.9**	–	Pyruvate dehydrogenase E1 β	260/6/6	22	44.7/5.9	38.6/5.3	
20	Q9S7W4	At3g07720	–	–	–	**4.4**	**2.7**	Galactose oxidase	290/5/5	18	36.0/5.1	35.8/5.1	
21	Q9SAJ4	At1g79550	–	–	**3.8**	–	–	Phosphoglycerate kinase	908/43/17	54	42.2/5.5	39.2/5.8	
22	Q9SAU2	At5g61410	–	**–4.7**	–	–	–	D-Ribulose-5-P-3-epimerase	377/16/8	29	30.1/8.2	22.1/6.9	
23	Q9M9K1	At3g08590	–	–3.9	–	–	–	Phosphoglyceromutase 2	734/16/15	41	60.9/5.5	67.2/6.1	Mn
24	Q7DLW9		–	–3.1	–	–	–	β-Fructosidase	669/14/12	18	73.8/5.4	51.7/5.3	
25	Q1WIQ6	At2g24270	–2.9	–	–	–	–	NADP-GAPDH	470/9/8	25	53.7/6.2	52.7/6.6	
26	Q94B07			–2.7	–	3.5	–	γ Hydroxybutyrate DH	632/14/12	41	30.9/5.9	28.0/6.1	
Photosynthesis													
27	O03042	AtCg00490	–	2.1	–	–	–	RuBisCO large subunit	1024/56/19	40	53.4/5.9	54.4/6.2	Mg
28	O49292	At1g77090	–3.6	–	–	–	–	OEC23-like protein 5	281/4/4	22	28.7/7.0	20.0/6.5	Ca
29	Q9ZR03	At4g03280	–	–	**–2.9**	–	–	Cytochrome *b6-f* complex Fe–sulphur subunit	112/3/2	10	22.8/8.6	14.9/6.4	Fe–S
30	Q9ZR03	At4g03280	–	–	–2.8	–	–	Cytochrome *b6-f* complex Fe–sulphur subunit	513/14/8	37	24.6/8.8	14.1/6.9	Fe–S
31	Q42029	At1g06680	–	–	**–2.5**	–	–	OEC protein 2-1	348/17/7	32	28.2/6.9	22.8/6.0	Ca

Table 4. Continued.

n	UniProt	AGI code	WT++ versus WT	*atfer* versus WT	*atfer*++ versus WT	*atfer*++ versus *atfer*	*atfer*++ versus WT++	Protein name/function	Sco/pep/ion	%	MW/pI th	MW/pI exp	Metal binding
Cofactor biosynthesis													
32	Q38814	At5g54770	–	–	–	**3.1**	–	Thiamine thiazole synthase	578/23/7	35	36.8/5.8	31.1/5.5	Fe
33	Q38814	At5g54770	–	–	–	2.5	–	Thiazole biosynthetic enzyme	645/22/9	33	36.8/5.8	29.6/6.0	Fe
34	O48588	At5g44720	–5.5	–6.6	–	–	–	MOCO sulphurase family protein	837/27/14	44	35.0/5.5	37.8/5.9	
Lipid metabolism													
35	O64968		–	–	–	2.4	–	Dihydrolipoylacyltransferase subunit of the AD complex	866/29/17	46	53.1/6.3	47.5/5.6	
36	Q93YW8	At4g18970	–	**–24.0**	**–5.8**	–	–	GDSL esterase/lipase	253/13/7	19	40.1/5.3	22.5/6.2	
37	Q93YW8	At4g18970	–	–	–	–	**–2.1**	GDSL esterase/lipase	403/8/6	16	70.9/8.2	35.2/5.5	
Stress													
38	Q8LBK6	At3g15660	–	**–15.4**	**–7.3**	–	–	Monothiol glutaredoxin-S15	200/7/5	38	18.8/5.2	12.2/4.8	Fe–S
39	P28493	At1g75040	–4.1	–	–	–	–	Pathogenesis-related protein 5	400/10/8	40	26.1/4.8	25.3/4.7	
40	Q96266	At2g47730	–6.4	–	–	–	**6.2**	Glutathione *S*-transferase-GST6	809/51/16	62	24.1/6.1	21.8/6.6	
41	Q9SJZ2	At2g22420	–	**–3.2**	–	**2.2**	–	Peroxidase 17	656/15/11	41	37.1/5.1	37.0/5.3	Fe–haem
DNA/RNA processes													
42	Q03250	At2g21660	–	**–7.5**	**ND**	–	–	Glycine-rich RNA-binding protein 7	378/9/6	43	16.9/5.8	11.0/6.3	
43	Q93W05	At1g10590	**–6.4**	–3.6	–	–	–	Replication factor A1	322/12/7	51	15.5/6.6	13.3/6.6	
44	Q9SMW7	At1g17880	–	**–2.1**	–	–	–	Basic transcription factor 3	249/8/6	47	17.9/6.6	16.0/6.7	
Cell cycle/biogenesis													
45	Q84M92	At1g18450	–	–	–	**2.4**	–	Actin-related protein 4	912/20/14	47	49.4/5.2	59.6/5.4	
46	P53494	At5g59370	–	–	**–3.2**	–	–	Actin 4	52/2/2	12	42.0/5.4		
47	Q42545	At5g55280	–	–2.4	–	**3.2**	–	Cell division protein FtsZ 1	756/22/14	29	45.8/6.9	36.7/5.2	
Cell wall organization													
48	Q9LJR7	At3g25050	–	–	–	–	**10.4**	Xyloglucan endotransglucosylase hydrolase protein 3	253/8/5	21	33.4/6.0	28.4/6.2	
49	Q9FLG1	At5g64570	–	–	–	ND		β-D-Xylosidase 4	522/10/9	18	85.3/7.8	60.4/6.2	
Secondary metabolism													
50	P94111	At1g74020	–	**ND**	–	New	–	Strictosidine synthase	581/14/10	41	35.6/6.0	35.6/6.0	
51	Q96330	At5g08640	–	–	–	–	**3.6**	Flavonol synthase	371/11/9	37	38.3/5.6	39.0/5.9	Fe
Others													
52	O80889	At2g32520	–	–	2.2	2.0	**3.6**	Carboxymethylenebutenolidase	344/9/6	45	26.0/5.3	24.8/5.4	Zn stress
53	Q9FMF2		–9.4	–	–	–	–	β-Ureidopropionase	424/9/6	21	45.6/6.0	43.2/6.5	
54	O64640	At2g45600	–	–	–6.7	–	–	Probable carboxylesterase 8	456/11/9	27	36.8/6.0	33.8/6.5	
55	Q42546	At5g63980	–	–	–2.1	–	–	SAL1 phosphatase	818/35/15	46	37.8/5.0	40.4/5.3	
Unknown													
56	Q8L768	At1g78150	–2.2	–	–	**–2.3**	–	Uncharacterized protein	773/16/13	46	29.7/6.2	30.1/6.6	
57	Q94EG6	At5g02240	–	–	2.3	–	–	Uncharacterized protein	277/8/5	20	41.9/6.0	20.1/5.5	
58	Q94EG6	At5g02240	–	2.4	–	–	–	Uncharacterized protein	873/27/14	60	27.1/6.2	27.3/6.4	
59	Q9LJE5	At3g13460	–	–3.6	–	–	–	Uncharacterized protein	500/8/8	16	72.7/5.7	93.0/6.1	
60	Q9SZP8	At4g38710	–	–	3.9	–	–	Glycine-rich protein	519/10/8	25	49.0/5.1	63.0/5.4	
61	Q941B7	At2g39730	–	–	2.1	**2.3**	**3.3**	At2g39730/T5I7.3	804/29/13		52.4/5.7	47.8/5.1	
62	Q94K71	At3g48415	–	–	–	**20.8**	–	Haloacid dehalogenase-like hydrolase domain-containing	805/22/15	45	34.7/8.3	27.6/5.4	
no ID													
63			–	–	–	3.1	–	No ID					

16% of the variability, with the second vector (v2) explaining 9% of the variability. The separation between clusters was associated with those metabolites with a large contribution (X-weight) to v1 (Supplementary Table S8). Approximately 70% of the metabolites with a high contribution to cluster separation were unknowns (Supplementary Table S8). The separation of the classes agreed with that found in the proteomic study, with *atfer1-3-4* and WT++ being closer together than WT and *atfer1-3-4*++.

A separate comparison was made between the triple ferritin mutant plants grown in Fe excess (*atfer1-3-4*++) with those of the same mutant grown in control conditions (*atfer1-3-4*). Fifteen identified metabolites and 21 unknowns showed significant changes between these two classes (Table 5). The largest changes in abundance were increases for urea, suberyl glycine, and proline (5-, 3-, and 2-fold, respectively). The unknowns accounted for 58% of the total metabolite changes. The clustering of metabolites was studied in each sample class using PLS analysis, including both the identified and unknown metabolites. The *atfer1-3-4* and *atfer1-3-4*++ classes were well separated in clusters, with the first vector (v1) explaining 28% of the variability, and the second vector (v2) explaining 14% of the variability (Supplementary Fig. S2C at *JXB* online). The metabolites with a large contribution (X-weight) to v1 are shown in Supplementary Table S9. Approximately 62% of the metabolites with a high contribution to cluster separation were unknowns (Supplementary Table S9).

A separate comparison was made between *atfer1-3-4*++ versus WT++. Four identified metabolites and seven unknowns showed significant changes between these two classes (Table 5). The largest changes in abundance were increases for urea, 2-hydroxyglutaric acid, and threonic acid (5-, 3-, and 2-fold, respectively), and decreases in threose (2-fold). The unknowns accounted for 64% of the total metabolite changes.

The information on the changes in metabolite abundances occurring in the different treatments was also clustered using Venn diagrams similar to those obtained for transcriptomic and proteomic data (Fig. 4). The category containing overlaps in the comparisons of *atfer1-3-4* versus WT, *atfer1-3-4*++ versus WT++, and *atfer1-3-4*++ versus WT has four metabolites: 2-hydroxyglutaric acid, threonic acid, and two unknowns. The second group of interest (only in *atfer1-3-4*++ versus WT++) contained four metabolites: threose and three unknowns. The third group of interest (only in *atfer1-3-4*++ versus WT) contained 23 metabolites: gluconic acid lactone, tyrosine, 3,6-anhydrogalactose, *N*-acetyl-D-hexosamine, salicin, ascorbic acid, and 17 unknowns.

Comparison of the flower hormonal profiles of Col-0 and atfer1-3-4 Arabidopsis *plants grown under iron-sufficient or excess conditions*

The *atfer1-3-4* mutant plants have their flower development severely impaired under Fe excess conditions (Ravet *et al.*, 2009*a*), suggesting some modifications in hormone concentration. The hormonal changes observed in this study between the two genotypes under two Fe conditions were restricted to the cytokinin concentrations, with the changes being especially intense in the mutant plants grown under Fe excess conditions. The IAA concentration in flower extracts was not significantly different in the *atfer1-3-4* and WT plants grown at both Fe levels. A similar conclusion can be drawn for the ABA concentrations in flower extracts (Table 6). In contrast, the concentrations of some cytokinins, including Z, tZR, cZR, and DHZR, showed significant changes (Table 6), whereas those of iPR did not change (the iP concentrations were below the limit of quantification; data not shown). The Z concentration in flowers was significantly higher in *atfer1-3-4*++ plants than in the other three plant classes, which had similar Z concentrations. On the other hand, similar tZR concentrations were observed in flowers from WT and mutant plants when grown under control conditions. However, the Fe excess treatment led to a significant and similar increase in the tZR concentration in flowers of both genotypes (Table 6). The cZR concentration was similar in flowers of WT, *atfer1-3-4*, and WT++ plants, but it was significantly lower in the flowers of *atfer1-3-4*++ plants. The DHZR concentration was lower in flowers of *atfer1-3-4* plants than in the WT plants, under both control conditions and Fe excess (Table 6). In flowers from WT plants, the DHZR concentration was lower with Fe excess, but the decrease was not statistically significant.

Discussion

The role of plastids in Fe homeostasis is an important parameter for normal flower development and for plant fertility. To document this point further, a global analysis (transcriptome, proteome, metabolome, and hormone concentrations) of *Arabidopsis* flowers from WT and triple *atfer1-3-4* ferritin mutant plants grown under control or Fe excess conditions was carried out. This approach proved to be valid based on the expression of the ferritin genes observed on the Affymetrix microarrays (Fig. 1C). The very low level of expression of the *AtFer1* and *AtFer4* genes in the flowers of the *atfer1-3-4* mutant plants confirms that these two genes were knocked out. On the other hand, only a mild decrease of the expression of the *AtFer3* gene in the *atfer1-3-4* mutant was observed when compared with WT plants under control conditions. This decrease in *AtFer3* transcript abundance becomes significant when the *atfer1-3-4* mutant plants are challenged with an excess of Fe. This result confirms that the *AtFer3* gene was knocked down, because a T-DNA insertion within its promoter region abolishes the regulation of its expression by Fe excess, but does not prevent its basal level of expression (Ravet *et al.*, 2009*a*). The robustness of the microarray analysis was further assessed by re-analysing 12 representative genes by qRT–PCR (Supplementary Table S1 at *JXB* online). Only one gene for one comparison showed deviating behaviour between qRT–PCR and microarray analysis.

Changes in gene expression at the transcript level because of mutations within ferritin genes and/or Fe excess treatment were low, with a total of 276 genes being significantly regulated (Fig. 1A, B; Table S5 at *JXB* online). Most fold changes observed in transcript abundance of these genes were not very

Table 5. Main changes in *Arabidopsis* flower metabolite levels. The corresponding response ratios, defined as the level in the WT++, *atfer1-3-4*, and *atfer1-3-4*++ classes divided by the level in the WT, are shown. When the response ratio was <1, the inverse was taken and the sign changed. Only metabolites showing changes in response ratios >1.5-fold and statistically significant (at $P \leq 0.05$) are included in the table.

	WT++ versus WT	***atfer1-3-4* versus WT**	***atfer1-3-4*++ versus WT**	***atfer1-3-4*++ versus *atfer1-3-4***	***atfer1-3-4*++ versus WT++**
Known metabolites					
Urea			9.8	4.9	4.7
Suberyl glycine				2.5	
2-Hydroxyglutaric acid		2.0	2.5		2.7
Proline				2.1	
Threonic acid		1.8	2.0		1.8
Gluconic acid lactone			2.0		
Homoglutamine		1.5	1.5		
Phenylalanine				1.5	
Tyrosine			–1.5		
Palmitic acid				–1.5	
Methylhexadecanoic acid				–1.5	
3,6-Anhydrogalactose			–1.6		
Heptadecanoic acid ester				–1.6	
Stearic acid				–1.6	
Levoglucosan				–1.6	
Glycerol				–1.6	
Glucose				–1.6	
N-Acetyl-D-hexosamine			–1.7	–1.7	
Pelargonic acid				–1.7	
Maltose				–1.8	
Malonic acid				–1.8	
Threose					–2.0
Salicin			–4.1		
Ascorbic acid	–4.8		–5.0		
Unknowns					
446831	12.5		20.6	19.5	
225867		3.8	3.8		3.0
310413		3.5	3.0		2.3
268365				2.7	
443451	2.4		2.5		
235436			2.3	2.4	
208850			2.0		
407649				1.9	
446856					1.9
212235			1.8		
446777					1.8
446849			1.8		
310006			1.7		
404568			1.6		
211956		1.6	1.6		
201005				1.6	
211932			1.5		
446884			1.5		
310006		1.5			
215062		1.5			1.5
211896			–1.5		
223865				–1.5	
214528				–1.5	
202834				–1.5	
446842				–1.5	
223629				–1.6	
204448				–1.6	
268353				–1.6	
231248				–1.6	

Table 5. Continued.

	WT++ versus WT	*atfer1-3-4* versus WT	*atfer1-3-4++* versus WT	*atfer1-3-4++* versus *atfer1-3-4*	*atfer1-3-4++* versus WT++
427262				–1.6	
299396				–1.6	
213194			–1.7		
447146			–1.8		–1.9
212251			–1.8		
446633				–1.8	
227724				–1.8	
217809			–1.9		
310785			–2.0		
213182				–2.2	
213198			–2.5	–1.9	
318412				–2.5	
213182					–2.5
305055			–2.6		
301584				–3.3	
222093		–3.7			
213230	–3.8	–3.1	–5.0		

high, ranging from 1.4- to 3.5-fold, with only a few strong alterations higher than 7-fold. Such a moderate quantitative impact of mutations and/or treatment was also observed for proteins (63 proteins with significant changes in relative abundance; Table 4) and metabolites (70 metabolites with significant changes in relative abundance; Table 5), with also a few strong alterations. Of the 63 protein spots identified by two-dimensional IEF in Table 4, 61 corresponding genes were represented on the ATH1 chip used for microarray analysis. When checking transcript signal values for these genes, only two of them [At1g06260, a cystein proteinase-like gene (CysP), and At3g25050, a xyloglucan endotransglucosylase (XTH3)] showed differential expression, which was significant for the *atfer1-3-4* versus WT comparison and elevated

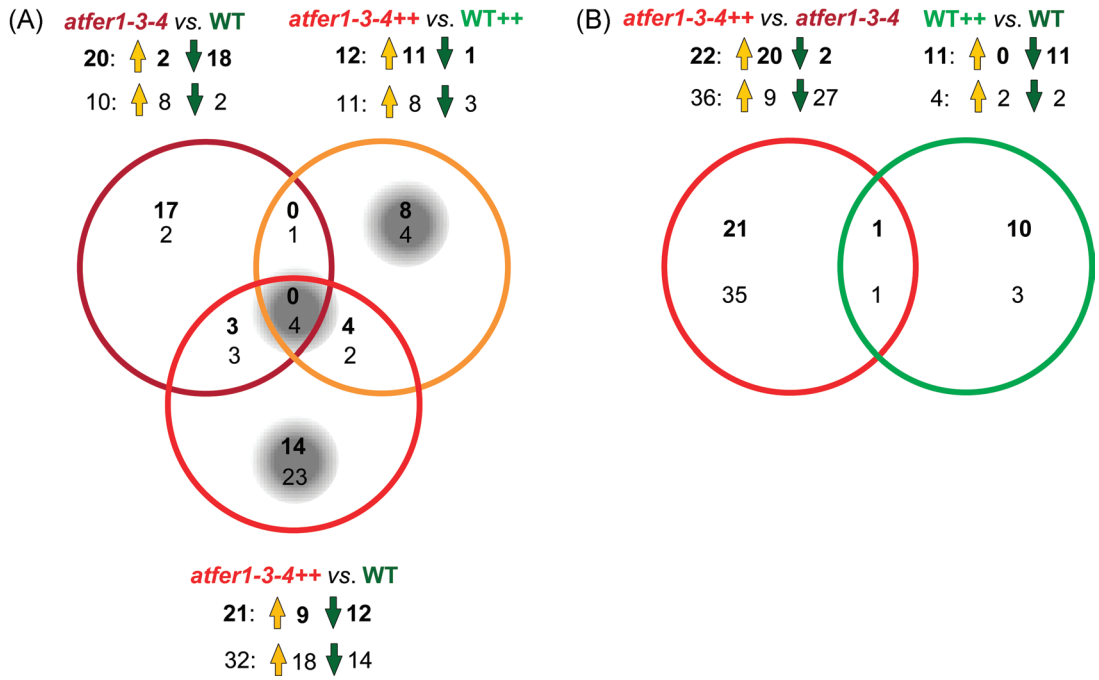

Fig. 4. Venn diagrams indicating major changes in *Arabidopsis* flower proteins and metabolites. Overlapping regulation is shown by Venn diagrams. Numbers indicate protein species (bold) and metabolites (regular) with significant and >2-fold changes in response ratios (i.e. abundance); up- and down-accumulation is indicated by orange and green arrows, respectively (for fold changes see Table 4). (A) Species showing differences in relative abundance in flowers of *atfer1-3-4* versus WT, *atfer1-3-4++* versus WT++, and *atfer1-3-4++* versus WT. Groups of interest discussed in the text are highlighted by a grey background. (B) Species showing differences in relative abundance in flowers of in *atfer1-3-4++* versus *atfer1-3-4* and WT++ versus WT.

Table 6. Hormone concentrations (IAA, ABA, Z, tZR, cZR, DHZR, and iPR) in flower extracts from Arabidopsis WT and atfer*1-3-4* plants grown in normal and Fe excess conditions. The results are presented as the means (for *n*=3) ±SD.

Hormone LQ (pmol g^{-1} FW)			***WT* (pmol g^{-1} FW)**	**atfer1-3-4 (pmol g^{-1} FW)**		**WT++ (pmol g^{-1} FW)**	***atfer1-3-4* ++ (pmol g^{-1} FW)**
IAA	3		77.76±3.11	79.85±12.84		81.68±14.62	76.18±6.66
ABA	1.5		165.10±16.16	170.99±49.83		147.07±29.09	137.39±39.24
Z	0.23		0.55±0.06	0.57±0.05		0.50±0.01	0.68±0.08
tZR	0.09		2.69±0.12	2.74±0.19		3.20±0.27	3.13±0.29
cZR	0.09		1.44±0.07	1.50±0.07		1.46±0.29	1.26±0.12
DHZR	0.28		0.45±0.08	0.29±0.11		0.33±0.15	BLQ
iPR	0.04		1.06±0.26	1.13±0.34		1.19±0.08	1.29±0.04
ANOVA source	IAA	ABA	Z	tZR	cZR	DHZR	iPR
Plant class	NS	NS	*	NS	NS	*	NS
Fe condition	NS	NS	NS	*	NS	NS	NS
Plant class×Fe condition	NS	NS	*	*	*	*	NS

WT, *Arabidopsis* Col-0 grown in normal conditions; *atfer1-3-4*, *Arabidopsis* mutant grown in normal conditions; WT++, *Arabidopsis* Col-0 grown in Fe excess; *atfer1-3-4++*, *Arabidopsis* mutant grown in Fe excess.

IAA, indole-3-acetic acid; ABA, abscisic acid; Z, *trans*-zeatin; tZR, *trans*-zeatin riboside; cZR, *cis*-zeatin riboside; DHZR, dihydrozeatin riboside; iPR, N^6-isopentenyladenosine; LQ, limit of quantification; BLQ, below the limit of quantification.

Statistical significance of the interaction among the different parameters: one-way ANOVA, LSD Fisher test (*significant differences $P \leq 0.05$).

for *atfer1-3-4*++ versus WT++. To verify transcriptomic data, mRNA contents of CysP and XTH3 were additionally analysed by qRT–PCR as described in Supplementary Table S1. Significance analysis by a Student's *t*-test revealed the same regulation as for DNA microarrays (data not shown). Overall, the multivariate statistical analysis (Supplementary Fig. S2) from proteomic and metabolomic data suggests that the mutant in control conditions clusters closely to WT plants grown in excess Fe, in agreement with the lower ferritin and higher Fe concentrations in flowers reported for this mutant (Ravet *et al.*, 2009*a*).

Functional categories consistently affected at the three levels of gene expression

In a recent study, Amiour *et al.* (2012) examined the impact of N deficiency in maize at the transcriptomic, proteomic, and metabolomic levels. These authors observed that integration of the three 'omics' studies was not straightforward, since different levels of regulation seem to occur in a stepwise manner from gene expression to metabolite accumulation. The same conclusion can be reached from the present study. Although no direct overlaps between transcripts, proteins, and metabolites were detected, some major modifications in specific functional categories were, however, consistently observed at these three levels of expression. The strongest impact concerns redox reactions and oxidative stress (i) with 70 transcripts of genes belonging to this functional category among the 276 affected (Fig. 1A, B; Supplementary Table S5 at *JXB* online); (ii) with changes in abundance of four proteins directly related to stress [monothiol glutaredoxin-S15, PR5, glutathione *S*-transferase (GST6), and peroxidase 17], and several oxidoreductases (Table 4); and (iii) with a decrease in ascorbic acid, which appears more dependent upon Fe excess treatment than upon the genotype considered (Table 5). These observations are consistent with the various flower phenotypes reported for *atfer1-3-4* plants (Ravet *et al.*, 2009*a*), which indicated that an Fe-mediated oxidative stress was enhanced when the ferritin Fe buffering capacity in chloroplasts was disturbed, ultimately leading to flower damage and fertility loss (Ravet *et al.*, 2009*a*; Briat *et al.*, 2010*b*). The second functional category being consistently affected at the three different levels of gene expression is related to amino acid and protein metabolism. The focus of regulated proteins in this category (Table 4) is well reflected by transcript regulation under Fe excess (*atfer1-3-4*++ versus WT++; Table 2). Proteolysis seems to play an important role, since genes coding for peptidase proteins are regulated (Tables 1, 2) and a cysteine proteinase-like protein (CysP) is synthesized *de novo* (100-fold increase) in the *atfer1-3-4* flowers from plants treated with excess Fe (Table 4). Indeed, analysis of the expression of the gene encoding CysP by qRT–PCR revealed increased transcript ratios in *atfer1-3-4* versus WT and *atfer1-3-4*++ versus WT++ (data not shown). Further, a new protein spot of a proteasome subunit, appearing in *atfer1-3-4*++ versus *atfer1-3-4* profiles (Table 4), points to protein degradation upon Fe stress in ferritin mutants. Because proteolysis-associated genes also represent targets for gene regulation in knockout and overexpressing mutants of the chloroplast Fe-transport protein PIC1 (Duy *et al.*, 2007, 2009), this functional category is closely linked to plastid Fe homeostasis and transport. At the metabolite level, the accumulation of urea (Table 5) is the ultimate marker of this activated proteolysis. Also consistent with changes in protein metabolism is the alteration in the pools of some amino acids such as tyrosine, phenylalanine, and proline in *atfer1-3-4* mutant plants treated or not with excess Fe (Table 5).

Influence of the ferritin mutation background on the flower-omes regardless of external iron feeding

The Venn diagrams (see shading in Figs 1A and 4A) show that the expression of 54 genes (Table 1) was changed, whereas no

proteins and only four metabolites were affected exclusively by the effect of the mutations. Among the genes affected, the stress and redox categories accounted for 28% of the changes. They also contained those genes showing the largest differences in expression. The majority of them showed up-regulation, some of them encoding Fe–haem oxidoreductases from the CYP family (cytochrome P450 superfamily), FAD berberine family, and two cell wall peroxidases. The substrate of CYP includes lipids, hormones, and xenobiotic substances, while the FAD-binding berberine family are, in general, membrane-associated oxidoreductases involved in electron transport, with both families usually being expressed during flower anthesis (TAIR annotation). The absence of haem proteins in the 2-DE study is probably related to the fact that most of them are membrane-located or cell wall-associated proteins, and therefore difficult to detect by this technique. Transcriptomic data also indicate that the impact of the mutations in the redox homeostasis processes occurs mainly at the membrane level. Regarding the metabolites found in this overlap, the increase in threonic acid, a product of ascorbic acid catabolism (Helsper and Loewus, 1982), would also suggest an increased redox stress. The increase in 2-hydroxyglutaric acid is also in agreement with the alterations caused by the mutant background, since it increases during senescence, when proteolysis and β-oxidation occur (Engqvist *et al.*, 2009, 2011).

Another category strongly affected by the mutations is hormone metabolism (Table 1), which shows a general up-regulation of genes responsive to ABA (At5g42560), ethylene (At1g36060, At3g50260), and auxin (At3g17600, At1g05680). The latter gene encodes a UDP-glucosyltransferase that acts on indole-3-butyric acid (therefore affecting auxin homeostasis), whose transcript and protein levels are strongly induced by H_2O_2, and which may allow integration of ROS and auxin signalling. In consonance with these results, it is worth mentioning that an additional target for gene regulation contained two transcription factors, At5g46350 (WRKY8) and At2g43000 (ANAC042, see Table 1), which are usually induced by the presence of H_2O_2, supporting the close connection between redox homeostasis and the mutant phenotype.

Impact of ferritin mutations on the flower-omes under iron excess in comparison with the wild type

The Venn diagrams also revealed 74 genes, eight proteins, and four metabolites differentially regulated only in *atfer1-3-4*++ versus WT++, which mainly reflect the consequences of excess Fe on the mutant (see shadings in Figs 1A, 4A; Tables 2, 4, 5). Among these genes, the specific increase in the FRO3 transcripts is surprising since it is described to be up-regulated in response to Fe deficiency. It may indicate amplified Fe(III) reduction activity and/or more transport and distribution of Fe. Targets for gene regulation in addition to the aforementioned proteolysis function also included the stress and redox and hormone metabolism categories. However, the effects of Fe excess (Table 2) were, in general, opposite to those exerted exclusively by the mutation regardless of the Fe status (Table 1). More specifically, FAD oxidoreductases and peroxidases were down-regulated, whereas CYP genes were still up-regulated. This different response of the Fe–haem proteins may point towards their different roles in the Fe and/or redox homeostasis mechanisms. In agreement with the transcriptomic data, two oxidoreductase proteins (spots 20 and 51) increased in abundance in the same comparison (Table 4). General stress responses represented by pathogenesis-related and disease resistance genes and by GST6 in the proteomic study (spot 40, Table 4) were also up-regulated. This up-regulation of stress responses, not observed in the WT, may indicate that *atfer1-3-4*++ flowers are facing more intense stress conditions than those of the WT++. In this comparison (Table 2), genes encoding hormone-responsive genes, similar to those up-regulated as a consequence of the mutations (Table 1), were down-regulated and included two auxin- (At1g19830, At2g46530) and two ethylene- (At1g63030, At5g52020) responsive genes. In addition, three of the proteins showing an increase in relative abundance in this group (spots 40, 48, and 51) are auxin regulated (UniProt DB annotation).

Adaptation of flower-omes representing an Fe effect on the ferritin mutant

Comparisons of *atfer1-3-4*++ versus WT showed changes in 43 transcripts, 14 proteins, and 23 metabolites (shading in Figs 1A, 4A, Tables 3, 4, 5), reflecting the Fe effect on the mutant. Besides the already described target categories for regulation, chloroplast-encoded genes are strongly regulated (Table 3; Supplementary S5 at *JXB* online) at the transcript level, especially in the *atfer1-3-4*++ versus WT comparison. This is consistent with three photosynthesis proteins affected (Table 4). It may indicate that pronounced imbalance in chloroplast Fe homeostasis by loss of the plastid Fe buffer ferritin, in parallel with excess external Fe supply, leads to the reprogramming of some chloroplast-intrinsic processes. Also, the strong decrease of salicin and ascorbic acid (Table 5), which are synthesized (salicin) and function as an antioxidant (ascorbic acid) in chloroplasts, might reflect disturbances of the plastid metabolism.

Cell wall and membrane biology modifications in response to ferritin mutations and/or Fe excess

Target categories for gene regulation by Fe excess on the mutant versus WT also included cell wall modification and transport, which accounted for 12% and 8% of the changes, respectively (Table 2). At the transcript level, a down-regulation was observed in genes encoding two pectin esterases and several structural components of the cell wall, including two expansins (EXPB4 and EXPA22), FLA12 (an arabinogalactan protein), and GRP5 (glycine-rich protein 5), whereas an up-regulation was observed in two extensins (At1g26240, At3g28550). At the protein level (Table 4), there was an increase in xyloglucan endotransglucosylase (spot 48), a cell wall-loosening enzyme thought to promote cell expansion (Fry *et al.*, 1992). When re-analysed by qRT–PCR, increased transcript ratios were found for the xyloglucan endotransglucosylase (XTH3) in *atfer1-3-4* versus WT and *atfer1-3-4*++ versus WT++ comparisons (data not shown). These changes

in cell wall structure may be behind the impaired fertility observed in the mutant, especially when grown with Fe excess. Furthermore, several of these genes are auxin responsive, and this might be directly related to the complex hormone balance commented on above.

Regarding transporter genes, 12 of them showed changes in regulation because of the *atfer1-3-4* mutations and/or Fe excess. Nitrate (*NTR1.1*) and phosphate (*PHT4.3*) transporters were up-regulated in the mutant background (Table 1), whereas an array of transporters were changed by Fe excess (Tables 2, 3), including several members of the ABC family (*ALS3*, *ABCG10*, and *ABC13*), a flavonoid antiporter (*TT12*), the amino acid (*CAT6*), malate (*ALMT1*), uracil (*UPS2*), and sugar (*ZIFL2*) transporters, and two transporters of unknown specificity (*DTX3* and *SEC14*). As expected from their membrane location, no transporters were found in the proteome analysis, whereas changes in the metabolome indeed reflected the changes in transporters described above. In particular, the increases in the relative abundance of amino acids (proline and phenylalanine) and the decreases in the relative abundances of sugars (maltose and glucose) would be in agreement with the increases observed in *CAT6* (amino acid transporter) and decreases in *ZIFL2* (sugar transporter) transcript abundances in the mutant. Further, the focus on regulation of transport-associated genes and the high overlap (about one-third, see Table 2) with genes also differentially expressed in PIC1ox lines (Duy *et al.*, 2011) indicate a close correlation between disturbance of Fe homeostasis and membrane transport. A strong deregulation of several transporters had already been reported in *atfer1-3-4* plants (Ravet *et al.*, 2009*a*). The present results are not fully consistent with previous results, with regard to the Fe(II) transporter IRT1 (Vert *et al.*, 2001), and the chloroplast iron permease PIC1 (Duy *et al.*, 2007). In the present microarray study, also confirmed by qPCR (data not shown), IRT1 and PIC1 did not show changes in expression between WT and *atfer1-3-4* plants, whereas IRT1 was found to be strongly down-regulated (Ravet *et al.*, 2009*a*) and PIC1 overexpressed (Duy *et al.*, 2007) in the *atfer1-3-4* mutant flowers. The reason(s) for such discrepancies is so far unknown.

Data discussed above indicate that mutations in ferritin genes exert an effect on redox enzymes, especially in those located in membranes, and that both ferritin mutations and Fe excess affect membrane transporters. These effects on membrane biology also correlate with changes observed in the lipid metabolism at the three omic levels. At the transcriptome level, the mutant background caused a decrease in a GDSL-motif lipase and in a lipid transferase (Table 1), which is consistent with the decreases measured in the relative amount of two GDSL lipases (spots 36 and 37, Table 4)

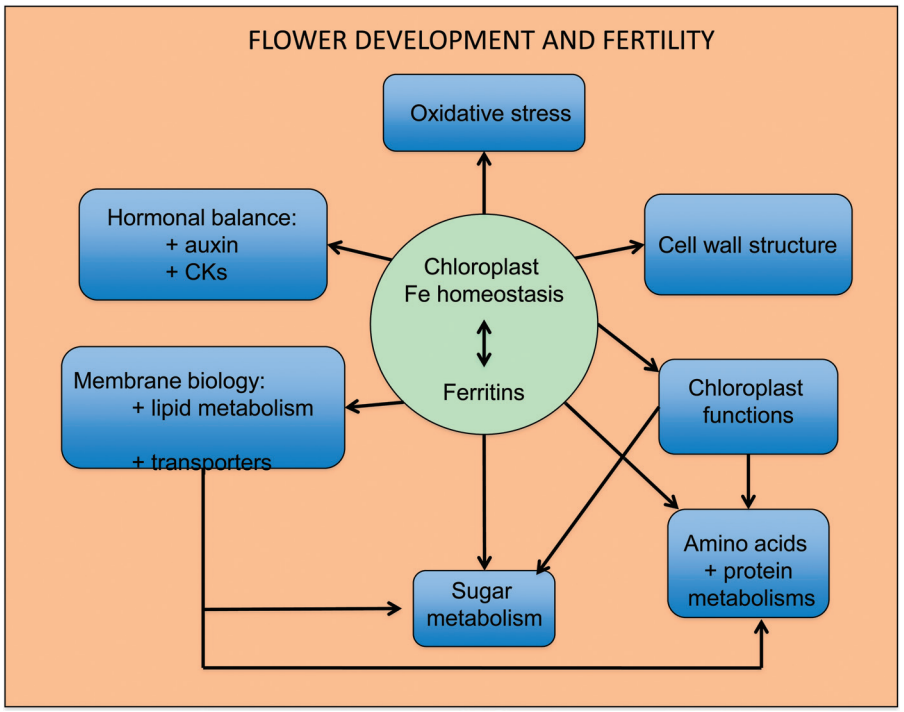

Fig. 5. Schematic representation of the biological functions bridging chloroplast Fe homeostasis to flower development and fertility. Disturbing Fe chloroplast homeostasis by altering the ferritin content promotes an oxidative stress and alters sugar, amino acid, and protein metabolism. This is consistent with the observation that chloroplast functions are perturbed, and that among transporters whose expression is altered in the *atfer1-3-4* ferritin mutant some of them are sugar and amino acid transporters. The membrane (lipid metabolism) and cell wall structure are also modified, as well as the hormonal balance, including cytokinins and perhaps auxins. This synthetic representation is based on the comparison (between Col-0 and the *atfer1-3-4* ferritin mutant plants grown under standard or excess Fe conditions) of the changes in the transcriptome, proteome, and metabolome occurring in the various functional categories defined in the text.

at the proteomic level, and at the metabolomic level with the changes in the pool of fatty acids (pelargonic, heptadecanoic, palmitic, and methyhexadecanoic acids), especially in *atfer1-3-4*++ versus *atfer1-3-4* (Table 5).

Hormonal imbalance in response to ferritin mutations and/or Fe excess

Among the various hormone concentrations measured in this study, only the concentration of active Z-based cytokinins was increased under Fe excess conditions in flowers of both genotypes (Table 6). This effect was more pronounced in flowers of *atfer1-3-4* mutant plants. Accordingly, in *atfer1-3-4*++ versus WT (Table 3), a down-regulation of the mitochondrial glutamate dehydrogenase (GDH3, At3g03910) was observed. This enzyme has been shown to be up-regulated in response to cytokinin and probably involved in control of nitrogen metabolism (Igarashi *et al.*, 2009), which also seems changed in the mutant, as indicated by the increase in urea in the *atfer1-3-4*++ versus WT and *atfer1-3-4* comparisons. A link between Fe homeostasis and cytokinins has already been reported for the regulation of the root Fe uptake system (Séguéla *et al.*, 2008). It is well known that the main active forms of cytokinins tended to concentrate in those plant organs that have high metabolic activity (Marschner, 1995; Sakakibara, 2006). The presence of cytokinins in these metabolic sites has a sink effect, attracting those metabolites and nutrients that are relevant to the development of intense metabolic activity (Marschner, 1995; Sakakibara *et al.*, 2006). In the context of the present experiments, the increase in concentration of Z-based active cytokinins in flowers suggests that Fe excess might increase the need for metabolites and nutrients in order to cope with the stress situation. Further, the up-regulation observed in nitrate and phosphate transporters in the mutant background would be in agreement with this hypothesis (Table 1). This situation seems to be more relevant in the case of *atfer1-3-4* mutant plants. This is supported by the fact that the increase in tZR is associated with a decrease in cZR, thus suggesting the conversion of cZR into tZR through the induction of *cis–trans* isomerase activity (Sakakibara *et al.*, 2006). Other hormones have been described to play a role in Fe metabolism, in particular auxin and ethylene (Bacaicoa *et al.*, 2011; Lingam *et al.*, 2011; Romera *et al.*, 2011; Giehl *et al.*, 2012), and also in flower functionality, as it is the case for gibberellins and IAA (Davies, 2004). Although a large number of genes and proteins regulated by these hormones had changed, the present study did not show any differences in the concentration of these plant hormones in flowers of both WT plants and *atfer1-3-4* mutant plants. However, since the analysis quantified the total hormone concentration, the possibility that conjugated forms or cellular distribution could be altered by Fe treatment cannot be excluded.

Influence of the Fe excess treatment on the flowerомes regardless of the genotype

Finally, six genes, one protein, and one metabolite responding to excess Fe irrespective of the genotype (common in the WT++ versus WT and *atfer1-3-4* ++ versus *atfer1-3-4* comparisons; Figs 1B, 4B) could be pinpointed. Among these genes, two encoded heat shock proteins and one a receptor kinase, and this is consistent with a stress situation. Unfortunately, two of these genes (At1g20070 and At1g76240, Table 3) and the protein (spot 56, Table 4) were of unknown function, and the metabolite (446831, Tables 4, 5) was also an unknown, but interestingly it was the one showing the largest change in the metabolomic study. These eight Fe-responsive elements are attractive targets for future studies dealing with the plant responses to Fe toxicity.

Conclusions

In conclusion, disturbing Fe homeostasis by mutations in ferritin genes and/or by Fe excess treatment leads to alteration of flower biology. This is reflected by changes in gene expression at the transcript and protein levels, as well as by modifications in various metabolite pools. Functional categories consistently affected at those three levels of gene expression were oxidative stress and protein metabolism. The mutant background caused alterations in Fe–haem redox proteins located in membranes, as denoted by changes in their transcript abundances and in hormone-responsive proteins (Fig. 5). The specific effect of excess Fe in the mutant caused further changes in these categories, suggesting that the mutant is facing a more intense Fe/redox stress. Changes in the membrane transporters and lipid metabolism (Fig. 5) also indicate that the impact of the mutation and/or Fe excess are very intense at the membrane level. In spite of the large number of genes and proteins responsive to hormones found to be regulated in this study, changes in the hormonal balance are restricted to cytokinin concentrations, being especially obvious in the mutant plants grown under Fe excess conditions. This reflects the complexity of the hormonal balance and the wide range of targets for hormone action in flower metabolism.

Supplementary data

Supplementary data are available at *JXB* online.

Figure S1. Protein species identified in extracts of *Arabidopsis* flowers.

Figure S2. Partial least square (PLS) analysis of *Arabidopsis* flower protein species and metabolites.

Table S1. Verification of DNA microarray data by quantitative RT–PCR.

Table S2. Overview of the metabolite reporting list.

Table S3. Optimal parameters for the detection of IAA and ABA used in the HPLC-ESI-MS/MS analysis of *Arabidopsis* plants.

Table S4. Optimal parameters for the multiple reaction monitoring detection of CKs used in the HPLC-ESI-MS/MS analysis of *Arabidopsis* plants.

Table S5. Genes significantly regulated in all five comparisons of *atfer1-3-4* mutants versus Col-0 wild type (WT) under Fe-sufficient and Fe-excess (++) conditions.

Table S6. Summary of the 2-DE protein profiling study results.

Table S7. Complete list of identified and unknown metabolites.

Table S8. Metabolite X-weights in the partial least square (PLS) analysis of *Arabidopsis* flowers shown in Supplementary Fig. S2.

Table S9. Metabolite X-weights in the partial least square (PLS) analysis of *atfer1-3-4* flowers shown in Supplementary Fig. S2.

Acknowledgements

We thank Professor Michael Grusak (BCM, Houston, TX) for his advice and careful reading and editing of the manuscript, and Karl Mayer (LMU München) for excellent technical assistance with microarray hybridization. This work was supported in the framework of the European Transnational Cooperation (Germany, France, Spain) within the PLANT-KBBE Initiative funded by (i) the Bundesministerium für Bildung und Forschung (BMBF, framework of the GABI initiative, FKZ:0315458A to KP), (ii) the Spanish Ministry of Economy and Competitivity (MINECO EUI2008-03618 to JA.) and (iii) the Agence Nationale de la Recherche (ANR-08-KBBE-009-01 to J-FB). The study was also supported by the MINECO grant AGL2010-16515 to JA.

References

Amiour N, Imbaud S, Clement G, *et al.* 2012. The use of metabolomics integrated with transcriptomic and proteomic studies for identifying key steps involved in the control of nitrogen metabolism in crops such as maize. *Journal of Experimental Botany* **63,** 5017–5033.

Bacaicoa E, Mora V, Zamarreño AM, Fuentes M, Casanova E, García-Mina JM. 2011. Auxin: a major player in the shoot-to-root regulation of root Fe-stress physiological responses to Fe deficiency in cucumber plants. *Plant Physiology and Biochemistry* **49,** 545–556.

Benjamini Y, Hochberg Y. 1995. Controlling the false discovery rate: a practical and powerful approach to multiple testing. *Journal of the Royal Statistical Society: Series B* **57,** 289–300.

Briat JF, Duc C, Ravet K, Gaymard F. 2010*a*. Ferritins and iron storage in plants. *Biochimica et Biophysica Acta* **1800,** 806–814.

Briat JF, Ravet K, Arnaud N, Duc C, Boucherez J, Touraine B, Cellier F, Gaymard F. 2010*b*. New insights into ferritin synthesis and function highlight a link between iron homeostasis and oxidative stress in plants. *Annals of Botany* **105,** 811–822.

Chich JF, David O, Villers F, Schaeffer B, Lutomski D, Huet S. 2007. Statistics for proteomics: experimental design and 2-DE differential analysis. *Journal of Chromatography B* **849,** 261–272.

Conte SS, Walker EL. 2011. Transporters contributing to iron trafficking in plants. *Molecular Plant* **4,** 464–476.

Curie C, Cassin G, Couch D, Divol F, Higuchi K, Le Jean M, Misson J, Schikora A, Czernic P, Mari S. 2009. Metal movement within the plant: contribution of nicotianamine and yellow stripe 1-like transporters. *Annals of Botany* **103,** 1–11.

Davies PJ. 2004. *Plant hormones* . Dordrecht: Kluwer Academic Publishers.

Dobrev PI, Kamínek M. 2002. Fast and efficient separation of cytokinins from auxin and abscisic acid and their purification using mixed-mode solid-phase extraction. *Journal of Chromatography A* **950,** 21–29.

Durrett TP, Gassmann W, Rogers EE. 2007. The FRD3-mediated efflux of citrate into the root vasculature is necessary for efficient iron translocation. *Plant Physiology* **144,** 197–205.

Duy D, Stübe R, Wanner G, Philippar K. 2011. The chloroplast permease PIC1 regulates plant growth and development by directing homeostasis and transport of iron. *Plant Physiology* **155,** 1709–1722.

Duy D, Wanner G, Meda AR, von Wirén N, Soll J, Philippar K. 2007. PIC1, an ancient permease in Arabidopsis chloroplasts, mediates iron transport. *The Plant Cell* **19,** 986–1006.

Engqvist M, Drincovich MF, Flügge UI, Maurino VG. 2009. Two D-2-hydroxy-acid dehydrogenases in Arabidopsis thaliana with catalytic capacities to participate in the last reactions of the methylglyoxal and beta-oxidation pathways. *Journal of Biological Chemistry* **284,** 25026–25037.

Engqvist MK, Kuhn A, Wienstroer J, Weber K, Jansen EE, Jakobs C, Weber AP, Maurino VG. 2011. Plant D-2-hydroxyglutarate dehydrogenase participates in the catabolism of lysine especially during senescence. *Journal of Biological Chemistry* **286,** 11382–11390.

Fernie AR, Aharoni A, Willmitzer L, Stitt M, Tohge T, Kopka J, Carroll AJ, Saito K, Fraser PD, DeLuca V. 2011. Recommendations for reporting metabolite data. *The Plant Cell* **23,** 2477–2482.

Fiehn O, Weckwerth W. 2003. Deciphering metabolic networks. *European Journal of Biochemistry* **270,** 579–588.

Fiehn O, Wohlgemuth G, Scholz M, Kind T, Lee do Y, Lu Y, Moon S, Nikolau B. 2008. Quality control for plant metabolomics: reporting MSI-compliant studies. *The Plant Journal* **53,** 691–704.

Fry SC, Smith RC, Renwick KF, Martin DJ, Hodge SK, Matthews KJ. 1992. Xyloglucan endotransglycosylase, a new wall-loosening enzyme activity from plants. *Biochemical Journal* **282,** 821–828.

Giehl RF, Lima JE, von Wirén N. 2012. Localized iron supply triggers lateral root elongation in Arabidopsis by altering the AUX1-mediated auxin distribution. *The Plant Cell* **24,** 33–49.

Helsper JP, Loewus FA. 1982. Metabolism of L-threonic acid in Rumex×acutus L. and Pelargonium crispum (L.) L'Hér. *Plant Physiology* **69,** 1365–1368.

Igarashi D, Izumi Y, Dokiya Y, Totsuka K, Fukusaki E, Ohsumi C. 2009. Reproductive organs regulate leaf nitrogen metabolism mediated by cytokinin signal. *Planta* **229,** 633–644.

Irizarry RA, Hobbs B, Collin F, Beazer-Barclay YD, Antonellis KJ, Scherf U, Speed TP. 2003. Exploration, normalization, and summaries of high density oligonucleotide array probe level data. *Biostatistics* **4,** 249–264.

Larsen PB, Geisler MJ, Jones CA, Williams KM, Cancel JD. 2005. ALS3 encodes a phloem-localized ABC transporter-like protein that is required for aluminum tolerance in Arabidopsis. *The Plant Journal* **41,** 353–363.

Le Jean M, Schikora A, Mari S, Briat JF, Curie C. 2005. A loss-of-function mutation in AtYSL1 reveals its role in iron and nicotianamine seed loading. *The Plant Journal* **44,** 769–782.

Lingam S, Mohrbacher J, Brumbarova T, Potuschak T, Fink-Straube C, Blondet E, Genschik P, Bauer P. 2011. Interaction between the bHLH transcription factor FIT and ETHYLENE INSENSITIVE3/ETHYLENE INSENSITIVE3-LIKE1 reveals molecular linkage between the regulation of iron acquisition and ethylene signalling in Arabidopsis. *The Plant Cell* **23,** 1815–1829.

Liu J, Luo X, Shaff J, Liang C, Jia X, Li Z, Magalhaes J, Kochian LV. 2012. A promoter-swap strategy between the AtALMT and AtMATE genes increased Arabidopsis aluminum resistance and improved carbon-use efficiency for aluminum resistance. *The Plant Journal* **71,** 327–337.

Liu J, Magalhaes JV, Shaff J, Kochian LV. 2009. Aluminum-activated citrate and malate transporters from the MATE and ALMT families function independently to confer Arabidopsis aluminum tolerance. *The Plant Journal* **57,** 389–399.

Lobréaux S, Hardy T, Briat JF. 1993. Abscisic acid is involved in the iron-induced synthesis of maize ferritin. *The EMBO Journal* **12,** 651–657.

Lohse M, Nunes-Nesi A, Krüger P, *et al.* 2010. Robin: an intuitive wizard application for R-based expression microarray quality assessment and analysis. *Plant Physiology* **153,** 642–651.

Marschner H. 1995. *Mineral nutrition of higher plants* . San Diego: Academic Press.

Maurer F, Müller S, Bauer P. 2011. Suppression of Fe deficiency gene expression by jasmonate. *Plant Physiology and Biochemistry* **49,** 530–536.

Mukherjee I, Campbell NH, Ash JS, Connolly EL. 2006. Expression profiling of the Arabidopsis ferric chelate reductase (FRO) gene family reveals differential regulation by iron and copper. *Planta* **223,** 1178–1190.

Ravet K, Touraine B, Boucherez J, Briat JF, Gaymard F, Cellier F. 2009*a*. Ferritins control interaction between iron homeostasis and oxidative stress in Arabidopsis. *The Plant Journal* **57,** 400–412.

Ravet K, Touraine B, Kim SA, Cellier F, Thomine S, Guerinot ML, Briat JF, Gaymard F. 2009*b*. Post-translational regulation of AtFER2 ferritin in response to intracellular iron trafficking during fruit development in Arabidopsis. *Molecular Plant* **2,** 1095–1106.

Rellán-Alvarez R, El-Hendoubi H, Wohlgemuth G, Abadía A, Fiehn O, Abadía J, Álvarez-Fernández A. 2011. Metabolite profile changes in xylem sap and leaf extracts of strategy I plants in response to iron deficiency and resupply. *Frontiers in Plant Sciences* **2,** 66.

Rellán-Alvarez R, Giner-Martínez-Sierra J, Orduna J, Orera I, Rodríguez-Castrillón JA, García-Alonso JI, Abadía J, Alvarez-Fernández A. 2010. Identification of a tri-iron(III), tri-citrate complex in the xylem sap of iron-deficient tomato resupplied with iron: new insights into plant iron long-distance transport. *Plant and Cell Physiology* **51,** 91–102.

Rodríguez-Celma J, Lattanzio G, Grusak M A, Abadía A, Abadía J, López-Millán A-F. 2011. Root responses of *Medicago truncatula* plants grown in two different iron deficiency conditions: analysis of the root protein profile and the riboflavin biosynthesis pathway. *Journal of Proteome Research* **10,** 2590–2601.

Rodríguez-Celma J, Lattanzio G, Jiménez S, Briat F, Abadía J, Abadía A, Gogorcena Y, López-Millán A-F. 2013. Changes induced by Fe deficiency and Fe resupply in the root protein profile of a peach–almond hybrid rootstock. *Journal of Proteome Research* **12,** 1162–1172.

Romera FJ, García MJ, Alcántara E, Pérez-Vicente R. 2011. Latest findings about the interplay of auxin, ethylene and nitric oxide in the regulation of Fe deficiency responses by Strategy I plants. *Plant Signaling and Behavior* **6,** 167–170.

Roschzttardtz H, Séguéla-Arnaud M, Briat JF, Vert G, Curie C. 2011. The FRD3 citrate effluxer promotes iron nutrition between symplastically disconnected tissues throughout Arabidopsis development. *The Plant Cell* **23,** 2725–2737.

Sakakibara H. 2006. Cytokinins: activity, biosynthesis, and translocation. *Annual Review of Plant Biology* **57,** 431–449.

Sakakibara H, Takei K, Hirose N. 2006. Interactions between nitrogen and cytokinin in the regulation of metabolism and development. *Trends in Plant Sciences* **11,** 440–448.

Schuler M, Rellán-Álvarez R, Fink-Straube C, Abadía J, Bauer P. 2012. Nicotianamine functions in the phloem-based transport of iron to sink organs, in pollen development and in pollen tube growth in Arabidopsis. *The Plant Cell* **24,** 2380–2400.

Schwacke R, Schneider A, van der Graaff E, Fischer K, Catoni E, Desimone M, Frommer WB, Flügge UI, Kunze R. 2003. ARAMEMNON, a novel database for Arabidopsis integral membrane proteins. *Plant Physiology* **131,** 16–26.

Séguéla M, Briat JF, Vert G, Curie C. 2008. Cytokinins negatively regulate the root iron uptake machinery in Arabidopsis through a growth-dependent pathway. *The Plant Journal* **55,** 289–300.

Smyth GK. 2004. Linear models and empirical Bayes methods for assessing differential expression in microarray experiments. *Statistical Applications in Genetics and Molecular Biology* **3**, Article 3.

Takahashi M, Terada Y, Nakai I, Nakanishi H, Yoshimura E, Mori S, Nishizawa NK. 2003. Role of nicotianamine in the intracellular delivery of metals and plant reproductive development. *The Plant Cell* **15,** 1263–1280.

Thimm O, Bläsing O, Gibon Y, Nagel A, Meyer S, Krüger P, Selbig J, Müller LA, Rhee SY, Stitt M. 2004. MAPMAN: a user-driven tool to display genomics data sets onto diagrams of metabolic pathways and other biological processes. *The Plant Journal* **37,** 914–939.

Vert G, Grotz N, Dédaldéchamp F, Gaymard F, Guerinot ML, Briat JF, Curie C. 2002. IRT1, an Arabidopsis transporter essential for iron uptake from the soil and for plant growth. *The Plant Cell* **14,** 1223–1233.

Waters BM, Chu HH, Didonato RJ, Roberts LA, Eisley RB, Lahner B, Salt DE, Walker EL. 2006. Mutations in Arabidopsis yellow stripe-like1 and yellow stripe-like3 reveal their roles in metal ion homeostasis and loading of metal ions in seeds. *Plant Physiology* **141,** 1446–1458.